Cell Reports

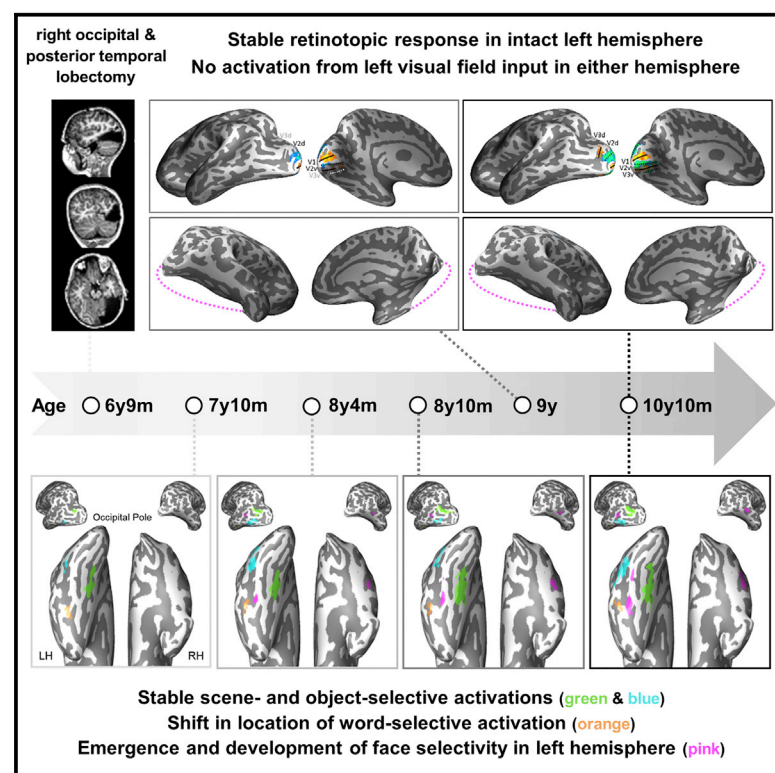# Successful Reorganization of Category-Selective Visual Cortex following Occipito-temporal Lobectomy in Childhood

Graphical Abstract

Highlights

- A 3-year longitudinal investigation of visual plasticity post lobectomy in a child

- Stable left homonymous hemianopia and no remapping of the early visual cortex

- Competition between face and word selectivity within a single (left) hemisphere

- Intact cognitive abilities and intermediate- and high-level visual function

Authors

Tina T. Liu, Adrian Nestor, Mark D. Vida, ..., Fan Nils Yang, Erez Freud, Marlene Behrmann

Correspondence

behrmann@cmu.edu

In Brief

Liu et al. present longitudinal behavioral and neuroimaging evidence tracking the development of and dynamic competition between face and word processing in a single (left) hemisphere following right occipito-temporal lobectomy in a young child. Normal intermediate and complex perception was evident, attesting to functional plasticity in the higher-order visual cortex.

CellPress

Successful Reorganization of Category-Selective Visual Cortex following Occipito-temporal Lobectomy in Childhood

Tina T. Liu,[1,2] Adrian Nestor,[3] Mark D. Vida,[1,2] John A. Pyles,[1,2] Christina Patterson,[4] Ying Yang,[1,5] Fan Nils Yang,[6,7] Erez Freud,[1,2] and Marlene Behrmann[1,2,8,*]
[1]Center for the Neural Basis of Cognition, Carnegie Mellon University and the University of Pittsburgh, Pittsburgh, PA, USA
[2]Department of Psychology, Carnegie Mellon University, Pittsburgh, PA, USA
[3]Department of Psychology, University of Toronto, Scarborough, Toronto, ON, Canada
[4]Department of Pediatrics, University of Pittsburgh, Pittsburgh, PA, USA
[5]Machine Learning Department, School of Computer Science, Carnegie Mellon University, Pittsburgh, PA, USA
[6]Department of Psychology, Sun Yat-Sen University, Guangzhou, China
[7]Center for Functional Neuroimaging & Department of Neurology, University of Pennsylvania, Philadelphia, PA, USA
[8]Lead Contact
*Correspondence: behrmann@cmu.edu
https://doi.org/10.1016/j.celrep.2018.06.099

SUMMARY

Investigations of functional (re)organization in children who have undergone large cortical resections offer a unique opportunity to elucidate the nature and extent of cortical plasticity. We report findings from a 3-year investigation of a child, U.D., who underwent surgical removal of the right occipital and posterior temporal lobes at age 6 years 9 months. Relative to controls, post-surgically, U.D. showed age-appropriate intellectual performance and visuoperceptual face and object recognition skills. Using fMRI at five different time points, we observed a persistent hemianopia and no visual field remapping. In category-selective visual cortices, however, object- and scene-selective regions in the intact left hemisphere were stable early on, but regions subserving face and word recognition emerged later and evinced competition for cortical representation. These findings reveal alterations in the selectivity and topography of category-selective regions when confined to a single hemisphere and provide insights into dynamic functional changes in extrastriate cortical architecture.

INTRODUCTION

The human ventral visual "what" pathway, projecting through the occipital pole to the anterior temporal lobe, comprises a host of category-selective areas. This topography follows a well-defined medial to lateral arrangement in adults and is highly reproducible across individuals (Grill-Spector and Weiner, 2014). Whether this cortical visual organization is fixed or, alternatively, plastic, is unclear. Examining the impact of surgical resection (e.g., lobectomy) and possible restitution of function can therefore offer unique insights into the (re)organization of the cortical visual system and mechanisms of functional recovery after brain injury. To date, little attention has been paid to the recovery of function following the resection of regions of the cortical visual system. Theoretically, one may postulate a continuum of possible outcomes ranging from no plasticity to complete reorganization. The extreme case of no reorganization is predicted by the hypothesis that the functional topographic map in the ventral cortex is innately prespecified (McKone et al., 2012) and that individual regions have a single assigned function (Kanwisher, 2010), which may be immutable. At the opposite extreme is the view that all brain areas are equipotent (Lashley, 1929), which predicts that many, perhaps even all, regions may plausibly assume the function of another region, and recovery ought to be complete. Of course, there are many other patterns of structure-functions correspondences that fall between these endpoints.

To assess the nature and extent of (re)organization of the residual visual cortex, we tracked the longitudinal changes in cortical organization in a pediatric case following surgical removal of the right ventral occipito-temporal cortex (VOTC) as a result of pharmacologically intractable epilepsy (Figures 1A and 1B). Pre-surgically, U.D. showed typical activation in the retinotopic cortex of both hemispheres and language was left lateralized (Figure S1A). Post-surgically, U.D. had a persistent left homonymous hemianopia as confirmed by two visual perimetry tests conducted 3 years apart (Figure 1C). Starting at 13 months post-surgery (age 7 years 10 months) and during the subsequent 36 months (age 10 years 10 months), U.D. was scanned five times and changes in functional selectivity and/or topography of the higher-order and early visual cortices were explored (Figure 1D). Psychophysics experiments were conducted in parallel to characterize any changes in visual behavior.

RESULTS

Topography and Selectivity of the Higher-Order Visual Cortex

Category-Selective Topography

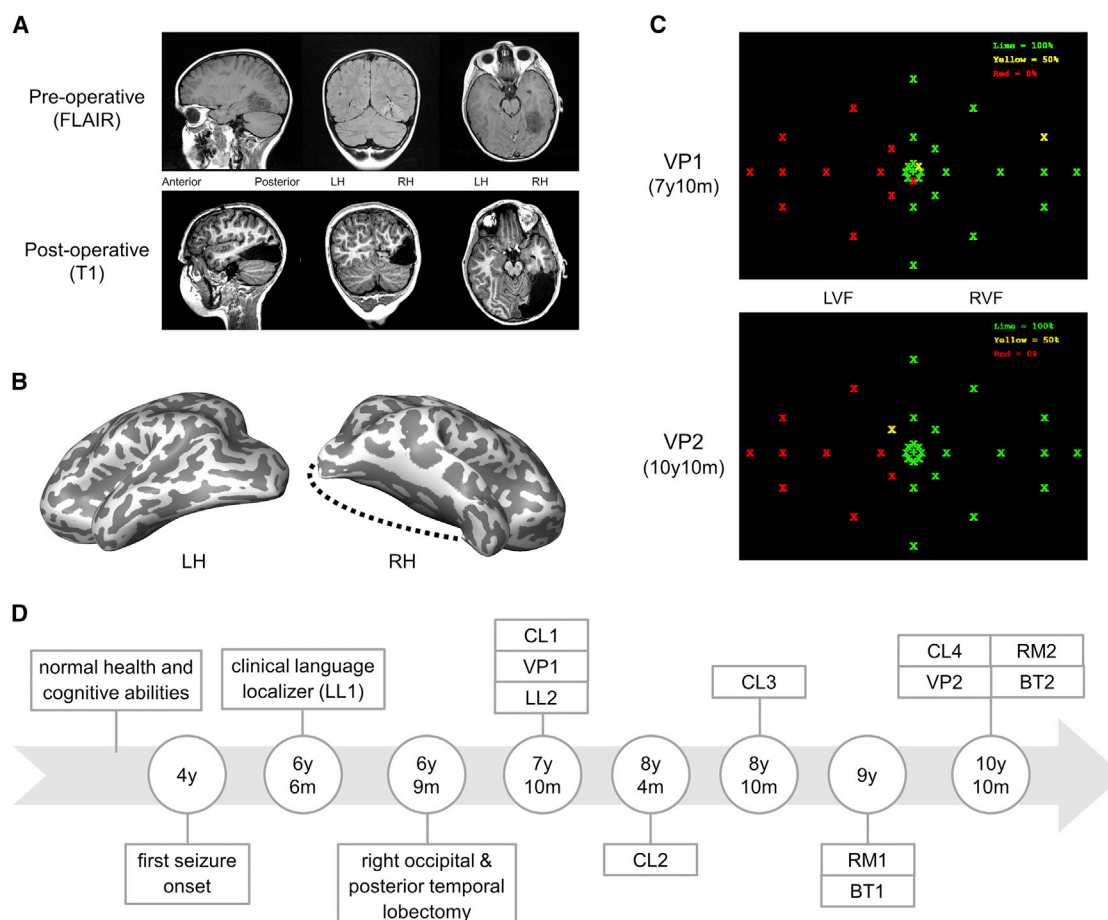We mapped regions preferentially responsive to different stimulus categories (faces, scenes, objects, and words; see

Figure 1. Patient Characteristics and Overview of the Longitudinal Investigation

(A) Pre-operative MRI shows the extent of the tumor (top), and post-operative MRI shows the outcome of the right occipital and posterior temporal lobectomy (bottom).

(B) Inflated cortical surface of both hemispheres post-resection. Black dotted line shows the boundaries of the resection.

(C) Two visual perimetry assessments post-surgery. Dots were presented twice in each location for detection. Severe visual field loss (two misses) in the left visual field (LVF) (red dots), full right visual field (RVF) (two hits) (green dots), and locations that were detected once (yellow dots).

(D) Timeline of the longitudinal investigation revealing the sequence of experiments: language localizer (LL), category localizer (CL), visual perimetry (VP), retinotopic mapping (RM), and behavioral testing (BT).

See also Figures S1 and S5 and Tables S1 and S2.

examples in Figure 2A) in U.D. (7 years 10 months–10 years 10 months) and in eight controls (7 years 5 months–11 years 5 months). Before the analyses, we carefully monitored and matched head motion and temporal signal-to-noise ratio (tSNR) in U.D. and controls (Figures 2D–2F) to ensure that any differences longitudinally or between U.D. and controls were not a result of differences in acquisition or data quality.

Category-selective responses are visualized in Figure 2B as a group selectivity map of all controls, the younger controls, and the older controls (two children, 8 years 11 months old, fell on different sides after a median split). Consistent with developmental studies (Golarai et al., 2007, Scherf et al., 2007), the topography in the controls consisted of bilateral face-selective activation in the fusiform face area (FFA; Kanwisher et al., 1997) and the posterior superior temporal sulcus (STS; Hoffman and Haxby, 2000), bilateral scene-selective

activation in the parahippocampal place area (PPA; Epstein and Kanwisher, 1998) and the transverse occipital sulcus (TOS; Nasr et al., 2011), bilateral object-selective activation in the lateral occipital complex (LOC; Malach et al., 1995), and left-lateralized word-selective activation in the visual word form area (VWFA; Cohen et al., 2000). That we were able to uncover robust topography of category selectivity both at the group and the individual levels in the controls attests to the sensitivity of the methods.

U.D.'s selectivity maps from category localizer 1 (CL1) to CL4 (7 years 10 months–10 years 10 months) are displayed in Figure 2C. Because of the right VOTC resection, most of the category-selective responses in U.D. were confined to the left hemisphere (LH), including left FFA (lFFA) and left STS (lSTS), left PPA (lPPA) and left TOS (lTOS), left LOC (lLOC), and left VWFA. In addition, U.D.'s right STS (rSTS), the only region that showed
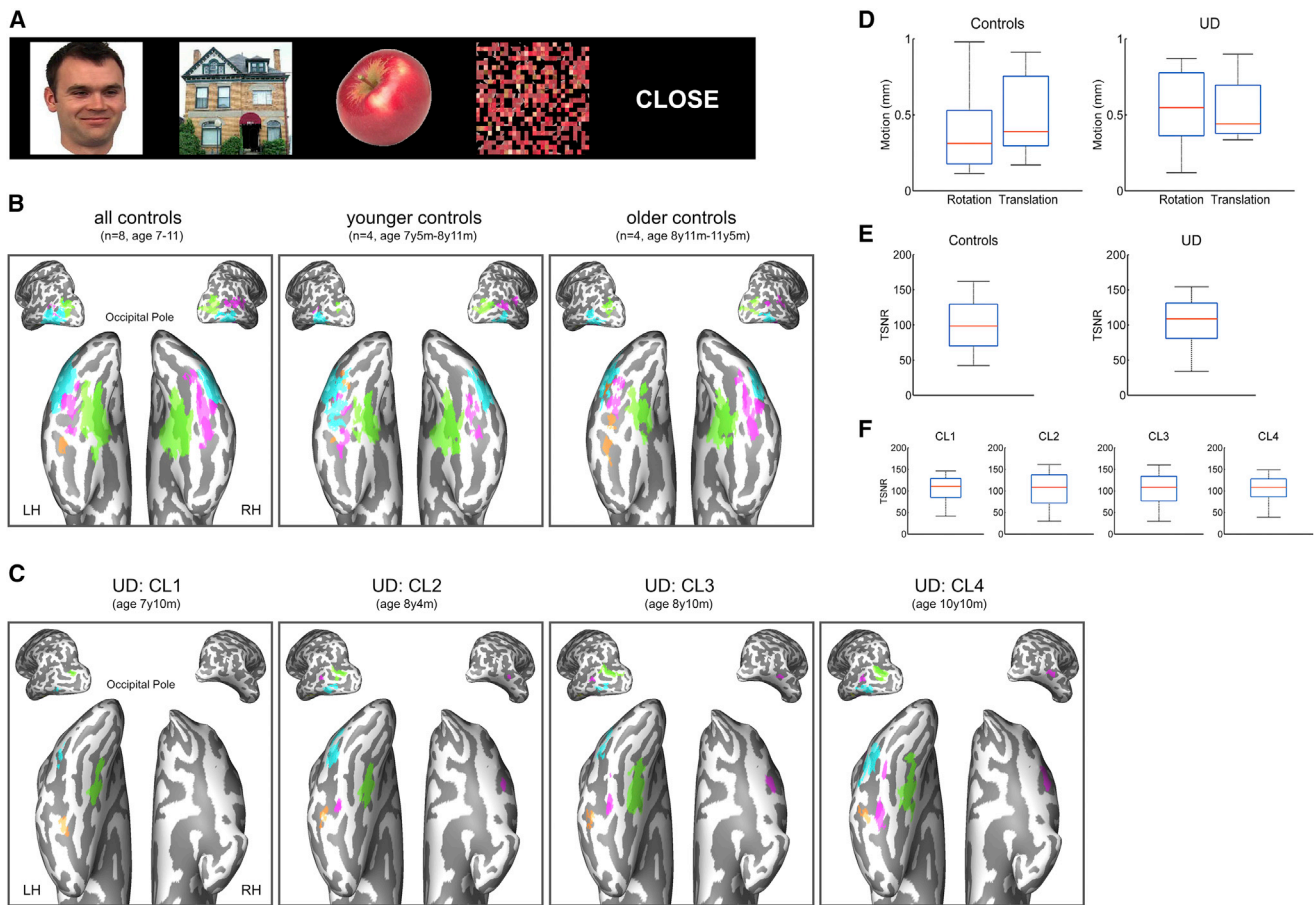
Figure 2. Category-Selective Activations, Head Motion, and tSNR in Controls and U.D.
(A) Examples of stimuli used in the fMRI category localizer (CL).
(B) Category-selective activations for all eight controls, four younger controls, and four older controls.
(C) Category-selective activations in U.D. from CL1 to CL4. Object-selective LOC (blue); scene-selective PPA and TOS (green); face-selective FFA and STS (pink); and word-selective VWFA (orange).
(D) Head motion in controls and U.D. The amounts of translation (in millimeters) and rotation (in degrees) in U.D. across four CL sessions were each within the control range.
(E) tSNRs in controls and U.D. tSNRs in U.D. across four CL sessions were each within the control range.
(F) tSNRs in each CL session in U.D. tSNRs were matched across the four sessions.
Each boxplot represents the median (red line), the 25% and 75% quartiles (length of the blue box), and the minimum and maximum values (black whiskers).

robust category selectivity (t > 3) in the right hemisphere (RH), showed selectivity for faces.

To quantify the stability of category-selective activations in U.D., we used Dice coefficients (Rombouts et al., 1997) to assess the degree of overlap in each region across sessions in a pairwise fashion (see STAR Methods). The results revealed that the object-selective lLOC and the scene-selective lPPA and lTOS were identified at reproducible locations across all four sessions (Figure 2C). The moderate-to-high degrees of overlap in these regions (R_{lPPA} = 0.73, threshold = 1440 voxels; R_{lTOS} = 0.61, threshold = 760 voxels; R_{lLOC} = 0.52, threshold = 1320 voxels) provides evidence of good test-retest reliability of longitudinal scans.

In contrast, there was minimal overlap in the word-selective VWFA activation across sessions (R_{VWFA} = 0.15, threshold =

300 voxels) and a lateral shift of the VWFA near the occipitotemporal sulcus from CL1 to CL3 (Figure 2C). The topography of face selectivity showed a mixed profile in which the activation remained stable in bilateral STS but was unstable in lFFA. Despite a lack of robust face selectivity in CL1, once face selectivity emerged in bilateral STS in CL2, its topography remained stable through CL4 (R_{lSTS} = 0.69, threshold = 540 voxels; R_{rSTS} = 0.58, threshold = 240 voxels). In contrast, a low Dice coefficient was found in the lFFA across three identifiable sessions (CL2–CL4; R_{lFFA} = 0.29, threshold = 200 voxels). The source of the two low Dice coefficients were, however, different. Distinct from the VWFA, in which there was a shift in the location of activation, the low Dice coefficient in the lFFA was the result of a significant increase in the number of lFFA voxels as a function of age (Figure S2A; R^2 = 0.99, p = 0.040).
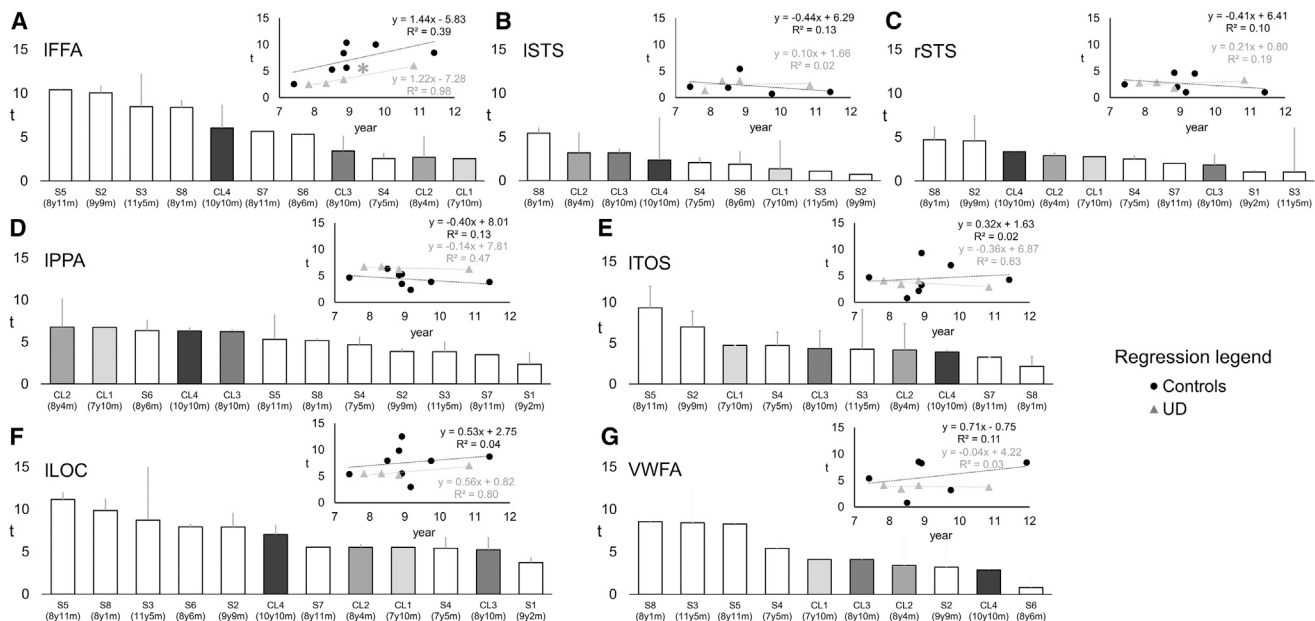
Figure 3. Category Selectivity in Controls and U.D.
(A–G) Category selectivity in controls and U.D. in (A) lFFA, (B) lSTS, (C) rSTS, (D) lPPA, (E) lTOS, (F) lLOC, and (G) VWFA.
Bar chart (main figure): Mean category selectivity (t value) in individual controls (white) and U.D. (different shades of gray for different sessions). Each white bar reflects data from a single control participant. The x axis is ranked in descending order to indicate where U.D. falls in the control distribution. Error bars indicate 1 SD between runs. Scatterplots (insets): Linear regression showing the relation between age (x axis) and category selectivity (y axis: t value) in controls (black) and in U.D. (gray). An asterisk (dark gray) is placed above the slope when there is a significant linear relation (lFFA). Number of ROIs defined in controls: lFFA (n = 7), lSTS (n = 5), rSTS (n = 6), lPPA (n = 8), lTOS (n = 6), lLOC (n = 8), and VWFA (n = 6).
See also Figure S2.

To evaluate whether U.D.'s category-selective topography and activation exhibited typical organization, we carried out three between-subject analyses comparing U.D. and controls. First, Crawford's modified t test (Crawford and Howell, 1998) on the spatial distribution of category-selective voxels revealed significant deviations in U.D.'s location of word-selective voxels in the center-of-mass X coordinate in CL3 and CL4 (controls: −40.89 ± 2.80; U.D. in CL3: −48.92, $t(6)$ = 2.683, p = 0.036; U.D. in CL4: −50.14, $t(6)$ = 3.090, p = 0.021), but not in any other category-selective regions or sessions (all t < 1.352, all p > 0.225), nor in any of the controls (all t < 1.898, all p > 0.090). Second, there were significantly fewer voxels in the lFFA in U.D. in the second session (CL2) compared to the age-matched controls ($t(6)$ = 2.498, p = 0.047), but not in other sessions or regions (all t < 2.087, all p > 0.05). Third, a linear regression analysis showed that the number of voxels as a function of age in each region of interest (ROI) in U.D. was not significantly different from that of the controls (95% CI; Weaver and Wuensch, 2013).

Magnitude of Category Selectivity
We then examined the magnitude of the selectivity in each region within U.D. over time and then evaluated whether U.D.'s developmental trajectory of category selectivity deviated from that of the controls. To avoid selection bias, category-selective ROIs were identified, using one run in each participant (see STAR Methods), which included lFFA (in 7/8 controls and in U.D.), lSTS (in 5/8 controls and in U.D.), rSTS (in 6/8 controls and in U.D.), lLOC (in 8/8 controls and in U.D.), lPPA (in 8/8 con-

trols and in U.D.), lTOS (in 6/8 controls and in U.D.), and VWFA (in 6/8 controls and U.D.).

Within U.D., there was a significant increase in face selectivity with age in the lFFA (Figure 3A, R^2 = 0.98, p = 0.008), but not in any other ROI (all R^2 < 0.80, all p > 0.05). Consistent with longitudinal studies of newborn monkeys in which early face selectivity was present in future face patches (Livingstone et al., 2017), the response of the future lFFA, lSTS, and rSTS (defined from run 1 in CL4) in CL1 showed early selectivity to faces (lFFA: t = 2.54, lSTS: t = 1.36, rSTS: t = 2.78), despite the absence of significant face-selective activations in CL1 (not robust at the t > 3 threshold; Figure 2C).

Next, we conducted three between-subject analyses to evaluate the magnitude, run-to-run variability, and development of category selectivity in U.D. compared to the controls (Figure 3). First, the magnitude of category selectivity in each session in U.D. was not significantly different from the mean selectivity of the age-matched controls (all t < 1.549, all p > 0.172). Second, the run-to-run variability in selectivity (SD between runs, error bars in Figure 3) in each session in U.D. was also not significantly different from that of the controls in any ROI (all t < 0.597, all p > 0.569). Third, the regression slope (selectivity as a function of age) in each ROI in U.D. (gray dashed lines in Figure 3) was within the 95% CI of that of the controls (black dashed lines in Figure 3), suggesting no significant deviation in U.D.'s development of category selectivity from that of the controls. The normality also held for the significantly positive lFFA

slope within U.D. (Figure 3A), which fell within the 95% CI of the controls' lFFA slope.

Relation between Faces and Words in the Left VOTC

We have visualized and analyzed the topography and magnitude of category selectivity across sessions in U.D. and compared his profile to that of the matched controls. Particularly intriguing is the visually salient lateral shift of VWFA (Figure 2C), the increase in magnitude (Figure 3) and size (Figure S2) of the lFFA, and the corresponding low Dice coefficient in these two regions across sessions. In typically developing individuals, there is differential hemispheric specialization for word and face representations (greater LH than RH activation for words and the converse pattern for faces). Because both words and faces have many visually confusable and homogeneous exemplars, these two visual classes, but not other classes, are thought to rely on regions of visual cortex with higher-acuity resolution (Levy et al., 2001).

However, because the image statistics of face and word exemplars are so dissimilar, it is thought that competition between word and face representations ensues during the course of literacy acquisition, with the result that word and face representations are localized to a greater degree in the LH and RH, respectively (Behrmann and Plaut, 2015; Dehaene et al., 2015). In U.D., in whom functional specialization was limited to one VOTC, we examined further the topographical relation between the VWFA and lFFA, with the prediction that the development in the lFFA (Figures 3A and S2A) and the change in topography of VWFA (Figure 2C) in U.D. may reflect experience-dependent plasticity under enhanced competition for neural resources. We tested this prediction using both univariate and multivariate analyses.

Within the joint anatomical ROI (FG + OTS) of fusiform gyrus (FG) and the occipitotemporal sulcus (OTS) (Figures 4A and 4B), a trend of encroachment of face-selective voxels and increase in face selectivity for previously non-selective voxels is evident across sessions (Figure 4C). The number of face-over-word selective voxels [$t_{(face-word)} > 0$] increased from 45.94% (CL1) to 47.99% (CL2) to 51.68% (CL3) to 67.43% (CL4). The binary change of selectivity [0 if $t_{(face-word)} \leq 0$, 1 if $t_{(face-word)} > 0$] at the voxel level was significant for each pair of sessions (McNemar's test of change, all $\chi^2 > 10.100$, all asymptotic p < 0.005), suggesting that the developing lFFA and adjacent VWFA in the left VOTC exhibited patterns that are consistent with reorganization resulting from competition.

Next, we computed the representational dissimilarity matrices (RDMs) to characterize the nature of the multivariate representations in the FG + OTS region (Figure 4D). The multidimensional scaling (MDS) plots (Figure 4E) reveal the similarity structure coded in the RDMs as distances between conditions in a 2D visualization. As apparent in the MDS plot, the different sessions of object and house conditions clustered together, whereas the distance between face and word conditions diverged over session. Using a bootstrap regression analysis (STAR Methods), a stable representation of houses and objects (Figure 4F [yellow dot]) was observed across sessions in the FG + OTS region (within 95% CI) and another control region (lateral occipital area 2 [LO2] [Wang et al., 2015]; Figure S3). In contrast, a dynamic relation between face and word representations (Figure 4F [red dot]) in the FG + OTS was evident across sessions (outside

95% CI) (see Figures S3C–S3E for a stable representation of faces and words in the control region).

Stable Topography in the Early Visual Cortex

Although our focus has been primarily on the remapping of category-selective cortex, we also evaluated the integrity of early visual cortex in U.D. Meridian mapping in retinotopic mapping 1 (RM1) and RM2 (1 year 10 months apart; see STAR Methods) revealed typical retinotopic maps in U.D.'s intact LH, with greater responses to stimulation along the horizontal meridian (solid lines) shown in orange and yellow and greater responses to stimulation along the vertical meridians (dashed lines) shown in blue and green (Figure 5).

Pre-surgically, stimulation in the LVF resulted in normal activation of the RH (Figure S1A). In neither post-surgical session was there a response to retinotopic stimulation in the RH under relevant contrasts (Figures 5D and 5E, S4D1, S4E1, S4D2, and S4E2), indicating no remapping of the left visual field to the ipsilateral hemisphere after resection of the right early visual cortex. More important, there was also no response to visual stimulation in the left visual field (LVF) in the intact LH in either session (Figures S4B2 and S4C2). This absence of activation from LVF input was consistent with the persistent left homonymous hemianopia (Figure 1C) and indicates that U.D.'s normal perception measured post-surgically (Figure S5; Table S1) was likely mediated solely by the residual left visual cortex.

Age-Appropriate Cognitive and Perceptual Performance

U.D.'s neuropsychological and scholastic records pre- and post-surgery (Table S2) revealed age-appropriate cognitive performance (IQ 116 and 118). To evaluate his visual behavior, on two separate behavioral testing (BT) sessions (1 year 10 months apart), relative to 14 age-matched controls, we compared his ability to perceive global forms (i.e., contour integration and Glass pattern), recognize faces, and discriminate objects (Figure S5).

U.D.'s psychophysical thresholds for the contour integration task (Hadad et al., 2010) fell within the normal range in both the aligned (BT1: $t(13) = 0.277$, p = 0.786; BT2: $t(13) = 0.867$, p = 0.402; Crawford's modified t test) and 20° misaligned condition (BT1: $t(13) = 0.416$, p = 0.684; BT2: $t(13) = 0.398$, p = 0.697; Crawford's modified t test) on both sessions (Table S1). His threshold for detecting the presence of Glass patterns (Lewis et al., 2002) was in the normal range at BT1 but was significantly better than the controls' threshold at BT2 (BT1: $t(13) = 1.727$, p = 0.108; BT2: $t(13) = 2.774$, p = 0.016; Crawford's modified t test) (Table S1). Given that the early visual cortex contributes to the perception of contours and Glass patterns (Field et al., 1993; Smith et al., 2002), these results implicate U.D.'s residual left visual cortex as the source of his normal performance.

U.D.'s object discrimination performance, measured in a speeded same/different task (Gauthier et al., 1999), fell within the normal range in both sessions (controls: accuracy = 88.6% ± 5.9%, inverse efficiency = 1366.4 ± 321.0; BT1: accuracy = 89%, inverse efficiency = 1116.8; BT2: accuracy = 91%, inverse efficiency score = 1502.2; p > 0.05; Crawford's modified t test) (Table S1).
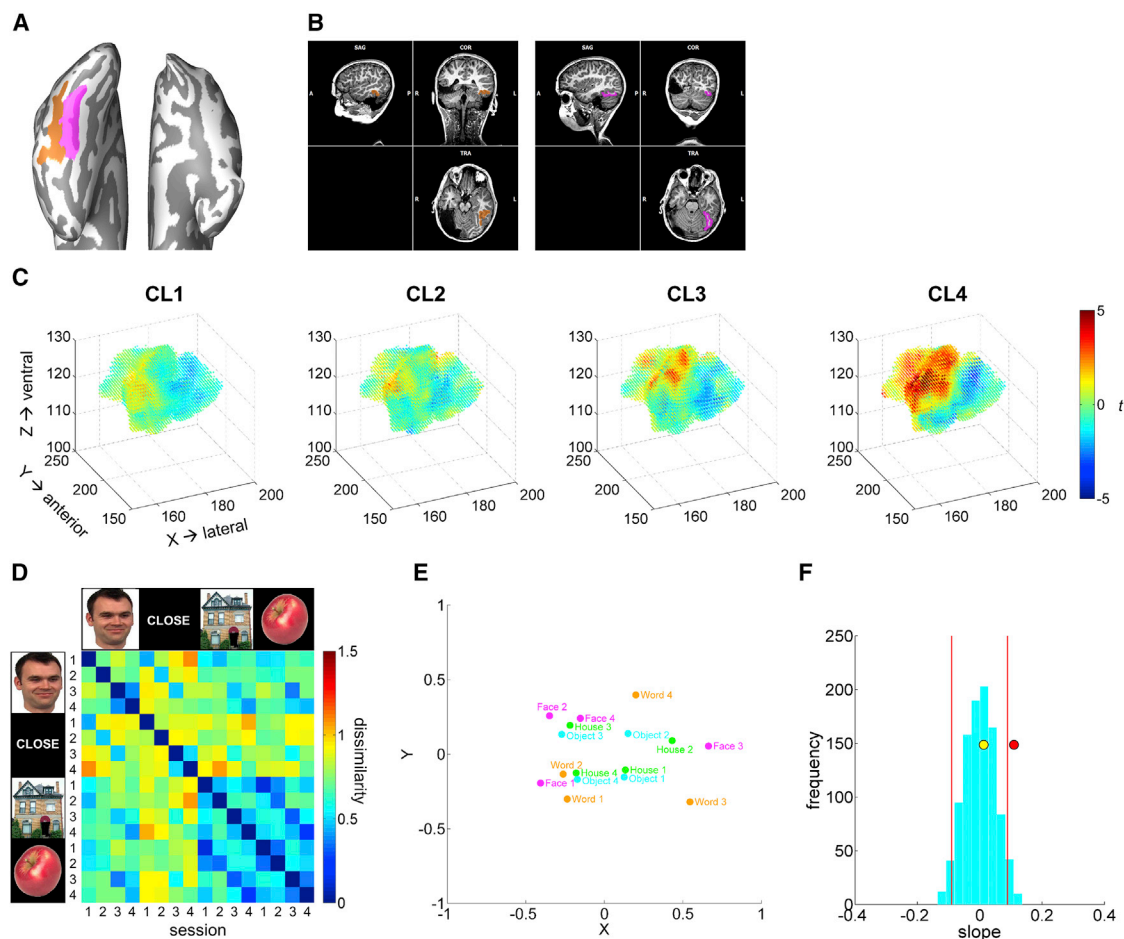
Figure 4. Results from the Anatomical ROI (FG + OTS) Analysis

(A) FG (pink) and OTS (orange) hand drawn in the surface space.

(B) FG (pink) and OTS (orange) in the corresponding volume space.

(C) Change over time in each voxel's selectivity to faces over words within the FG + OTS region, where the XYZ coordinates (in native space) and the t score [$t_{(face-word)}$] are plotted for each voxel. Higher sensitivity to faces (dark red); higher sensitivity to words (dark blue).

(D) Representational dissimilarity of category representations across sessions in the FG + OTS region.

(E) MDS plot of category representations across sessions in the FG + OTS region. Words (orange), faces (pink), houses (green), objects (blue).

(F) A distribution of bootstrapped dissimilarity slopes (cyan histogram), face and word dissimilarity slope (red dot), and house and object dissimilarity slope (yellow dot) as a function of session. 95% CI (red vertical lines).

See also Figure S3.

In both sessions, U.D.'s face recognition ability, measured using the Cambridge Face Memory Test for Children (CFMT-C; Croydon et al., 2014), fell within the normal range of the control sample from Croydon et al. (2014) (BT1 compared to 9-year-olds: n = 33, $t(32)$ = 0.540, p = 0.593; BT2 compared to 11-year-olds: n = 29, $t(28)$ = 0.014, p = 0.989, Crawford's modified t test). Pre-surgical neuropsychological evaluation at age 6 years 6 months (3 months before surgery) documented performance within the high average range in face memory (scaled score = 13 in A Developmental Neuropsychological Assessment-II [NEPSY-II] Memory for Faces subtest).

U.D.'s reading comprehension, assessed using the Clinical Evaluation of Language Fundamentals-Fifth Edition (CELF-5), at BT2 revealed above-average performance in his age range

(scaled score = 19, mean = 10, 3 SD above mean). His scholastic records and neuropsychological evaluations also documented above-average to proficient reading both before and after surgery (Table S2).

DISCUSSION

In this study, we offer a 3-year longitudinal examination of the extent and nature of reorganization of the visual system in a child, U.D., who underwent a right occipital and posterior temporal lobectomy at age 6 years 9 months. Using both behavioral and neuroimaging approaches, we characterized the status and changes in early and extrastriate visual cortices, evaluated visuoperceptual performance, and assessed the extent to which
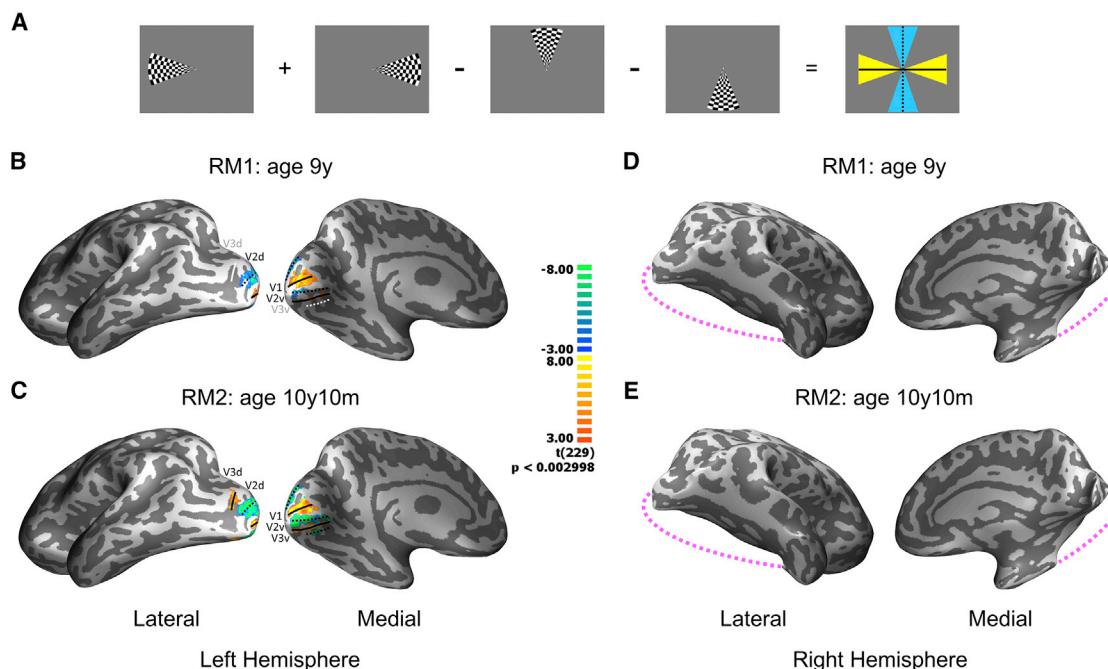
Figure 5. Early Visual Cortex Activation in U.D. in RM1 (Age 9 Years) and RM2 (Age 10 Years 10 Months)
(A) Stimuli and contrasts used in the retinotopic mapping experiment. This image shows a contrast between horizontal meridian (LVF + RVF) and vertical meridian (upper VF + lower VF).
(B) Retinotopic response in the LH in RM1.
(C) Retinotopic response in the LH in RM2.
(D) Retinotopic response in the RH in RM1.
(E) Retinotopic response in the RH in RM2.
Stronger responses to stimulation along the horizontal meridian (yellow and orange); stronger responses to stimulation along the vertical meridians (blue and green). All meridians were defined in RM2 and placed by point-by-point correspondence on top of RM1.
Horizontal meridians (solid black lines); vertical meridians (dashed black lines); meridian identified in RM2 but not in RM1 (V3d and V3v; white lines); and resection in the right hemisphere (pink dashed lines). Color scale bars represent t scores.
See also Figure S4.

the reorganized visual system obeyed the normal developmental profile.

Several major findings emerged. First, there was no reorganization of the early visual cortex, and U.D. evinced persistent left hemianopia and no activation associated with stimulation in the hemianopic visual field (Figures 5 and S4), despite normal bilateral contralateral activation pre-surgically (Figure S1A). Second, two patterns were observed in category-selective regions: (1) in regions such as lPPA and lTOS, category selectivity was present from the first post-surgical scan, and the topography, extent, and selectivity of these regions fell within the normal distribution and did not change longitudinally (Figures 2, 3, and S2), and (2) the activation pattern of other regions such as the VWFA and the lFFA changed over time, with the location of the VWFA shifting and the extent of the lFFA expanding (Figures 2C and S2A).

Moreover, univariate and multivariate analyses revealed that the proximal VWFA and lFFA regions became less similar over time (Figure 4), perhaps reflecting competition for representational space in the residual left VOTC. Notwithstanding the dynamic changes in VOTC, the developmental trajectory of these two regions was not differentiable from the trajectory of normal development, as measured by the slope of size and the slope

of category selectivity as a function of age. Finally, consistent with the normal developmental trajectory, U.D.'s performance in tasks tapping intermediate- and high-level visual computations fell entirely within normal limits (Table S1). The dramatic findings of essentially normal perceptual behavior and normal (albeit rearranged) neural correlates, confirmed by converging analytic methods (univariate, multivariate) and multiple dependent measures (Dice coefficients, number of voxels, selectivity), attest to the power of plasticity of the higher-order visual system.

We also confirmed that any observed changes in topography and selectivity were not artifacts of the test-retest scanning procedures. We matched the head motion and tSNR across sessions and participants (Figures 2D–2F), and our analytic approach relied primarily on weighted contrasts rather than on absolute response amplitudes. In addition, high Dice coefficients were derived from session to session from the activation profile for some regions (e.g., lPPA, lSTS), attesting to the stability of the data. These careful controls ensure that the observed alterations in topography and selectivity are the veridical product of remapping rather than the outcome of variability in data acquisition. Our data present a systematic longitudinal investigation of visual behavior and neural responses post-lobectomy in childhood and

offer a window into the microgenesis of change in the visual system.

Persistent Hemianopia and No Change over Time

There was no evidence of remapping in early visual areas, and U.D. evinced a persistent left hemianopia across all of the sessions. While both early and secondary visual areas in both hemispheres were activated in pre-surgery imaging (Figure S1A), no activation from stimulation of the LVF was observed in either hemisphere post-surgery (Figures S4B2–S4E2). The absence of visual field recovery is compatible with persistent contralateral hemianopia following hemispherectomy (Ptito and Leh, 2007) or visual deprivation (Crair et al., 1998), which indicate that the topography of the early visual cortex may be established and fixed at an early age.

Stability Versus Functional (Re)organization in Intact Cortex

In regions whose category-selective emergence typically occurs earlier in development and whose cortical pattern is not typically lateralized to one hemisphere (e.g., lLOC, lPPA), U.D.'s spatial topography followed the normal developmental profile, and this topography remained stable across all of the sessions. In contrast, plasticity was observed in regions that are associated with a protracted developmental trajectory (Golarai et al., 2007; Scherf et al., 2007) and hemispheric superiority. For example, although face lateralization to the LH is less typical in normal participants, there was a significant increase in the magnitude and extent of activation in U.D.'s lFFA across sessions (Figures 3 and S2).

Furthermore, this atypical FFA lateralization appears to have affected the word-selective LH region such that (1) a dynamic shift in the VWFA activation over time was observed (Figure 2C), (2) face selectivity encroached into the center of the FG + OTS region (Figure 4C), and (3) the MDS distance between face and word increased over session in the FG + OTS region (Figure 4E). In addition to the competition between word and face representations (because of foveal bias; Levy et al., 2001) during literacy acquisition (Behrmann and Plaut, 2015; Dehaene et al., 2015), the outcome described here may be critical for optimizing connectivity and maintaining separability of representation (Grill-Spector and Weiner, 2014). Taken together, the present results provide strong support for the plasticity of both face and word selectivity under constraints for neural resources.

Normal Visual Recognition in the Absence of the Right Ventral Visual Pathway

Attesting to the functionality of the reorganization of the category-selective cortex, no visual impairments (except persistent hemianopia) were uncovered, even with fine-grained psychophysical measures (Figure S5; Table S1). It is also worth noting that, although fMRI results indicate a competition between face and word selectivity within the adjacent cortex, we have no behavioral evidence to suggest that either word or face recognition is compromised as a result of face lateralization to the same (LH) hemisphere. Given that limited recovery has been noted in individuals with a lesion or resection of the visual cortex early in life (Farah et al., 2000), it is striking that U.D. had normal face recognition, as well as form and object perception.

The absence of prosopagnosia in U.D. challenges the importance of the right ventral visual pathway in face processing (Kanwisher, 2010) and the evidence that the right VOTC damage may be sufficient to produce prosopagnosia (De Renzi, 1986). U.D.'s normal face recognition also challenges the conclusion that face selectivity and its anatomical localization is genetically coded and that subsequent compensation is not possible (Farah et al., 2000). In contrast, our results favor dynamic reorganization and fine-tuning in the functional architecture of cognition over development (Johnson, 2011) and argue for the critical role of experience in shaping the underlying circuitry (Arcaro et al., 2017).

What Factors Affect Plasticity?

In a recent review of VOTC damage in children, Liu and Behrmann (2017) noted that the majority of cases showed limited recovery and that their visual deficits tended to affect multiple stimulus categories. Clearly, this was not the case for U.D. As widely documented, there are many factors that predict the nature of post-surgical change. For example, better prognosis is predicted by a better pre-surgical cognitive profile, by more circumscribed cortical resection, and by chronic etiology. For example, a slow-growing tumor potentially affords greater opportunity for plasticity than an acute incident such as post-natal stroke (Mancini et al., 1994) or meningitis (Farah et al., 2000). Moreover, the earlier the resection the better (Bourne, 2010). Most of these factors weigh favorably in U.D.'s case and likely contribute to the positive outcome. However, as noted, reorganization is not ubiquitous and the pattern of reorganization may be contingent on region: in U.D., reorganization was restricted to regions with prolonged developmental emergence (e.g., VWFA, lFFA), while stability was observed in those regions with an earlier developmental emergence that was apparent even in the first post-surgical scan (e.g., lPPA, lTOS).

Although we can explicate the factors that predict better recovery, we do not yet have a definitive account of the exact neurobiological mechanisms that trigger and drive plasticity, nor do we have clear specifics on how the altered architecture is implemented. One possible mechanism may involve rerouting through the thalamus (Ajina et al., 2015), and subcortical structures may play an important role in reorganizing face recognition, given their role in bootstrapping cortex in the course of face perception in infancy (Johnson, 2005), continued engagement in face perception in adulthood (Gabay et al., 2014), and their phylogenetic role in face perception (Dyer et al., 2005). Another although not mutually exclusive possibility is that because face recognition is so complex and its developmental trajectory is protracted even into early adulthood (Germine et al., 2011), advantage can be taken of the continued growth of the neocortex itself with the addition of myelin, dendritic growth, non-neuronal cells, and a complex process of resculpting synapses present even into adolescence (Bei et al., 2016).

Our results indicate dynamic reorganization over time in the higher- but not the lower-order visual cortex following right posterior lobectomy. The longitudinal nature of our investigation offers important insights into the profile and extent of remapping cortical visual function. In particular, we detected persistent hemianopia, documented stable patterns in scene- and

object-selective cortex, and uncovered the development of and dynamic competition between face and word processing in the same hemisphere. Normal face perception was evident without the right ventral visual pathway, the pre-eminent regions involved in face recognition, attesting to the functional plasticity in the higher-order visual cortex. The present results shed light on the plasticity in the higher-order visual cortex in the context of severe anatomical perturbation and have implications for understanding the development of cognitive architecture and its functional selectivity more generally.

STAR★METHODS

Detailed methods are provided in the online version of this paper and include the following:

- KEY RESOURCES TABLE
- CONTACT FOR REAGENT AND RESOURCE SHARING
- EXPERIMENTAL MODEL AND SUBJECT DETAILS
  - Patient
  - Controls
- METHOD DETAILS
  - Stimuli and Procedures
  - fMRI Experiments
  - Scanning
  - Structural MRI
  - Functional MRI
- QUANTIFICATION AND STATISTICAL ANALYSIS
  - fMRI Data Analysis
- DATA AND SOFTWARE AVAILABILITY

SUPPLEMENTAL INFORMATION

Supplemental Information includes five figures and two tables and can be found with this article online at https://doi.org/10.1016/j.celrep.2018.06.099.

AUTHOR CONTRIBUTIONS

Conceptualization, A.N. and M.B.; Methodology, A.N., M.D.V., and J.A.P.; Investigation, T.T.L., M.D.V., and J.A.P.; Formal Analysis, T.T.L., F.N.Y., and A.N.; Software, Y.Y.; Writing – Original Draft, T.T.L. and M.B.; Writing – Review & Editing, T.T.L., M.D.V., J.A.P., Y.Y., A.N., E.F., and M.B.; Visualization, E.F.; Funding Acquisition, A.N. and M.B.; Resources, C.P.; Supervision, M.B.

DECLARATION OF INTERESTS

The authors declare no competing interests.

REFERENCES

Ajina, S., Pestilli, F., Rokem, A., Kennard, C., and Bridge, H. (2015). Human blindsight is mediated by an intact geniculo-extrastriate pathway. eLife 4, 164–178.

Arcaro, M.J., Schade, P.F., Vincent, J.L., Ponce, C.R., and Livingstone, M.S. (2017). Seeing faces is necessary for face-domain formation. Nat. Neurosci. 20, 1404–1412.

Behrmann, M., and Plaut, D.C. (2015). A vision of graded hemispheric specialization. Ann. N.Y. Acad. Sci. 1359, 30–46.

Bei, F., Lee, H.H.C., Liu, X., Gunner, G., Jin, H., Ma, L., Wang, C., Hou, L., Hensch, T.K., Frank, E., et al. (2016). Restoration of visual function by enhancing conduction in regenerated axons. Cell 164, 219–232.

Bourne, J.A. (2010). Unravelling the development of the visual cortex: implications for plasticity and repair. J. Anat. 217, 449–468.

Cohen, L., Dehaene, S., Naccache, L., Lehéricy, S., Dehaene-Lambertz, G., Hénaff, M.-A., and Michel, F. (2000). The visual word form area: spatial and temporal characterization of an initial stage of reading in normal subjects and posterior split-brain patients. Brain 123, 291–307.

Crair, M.C., Gillespie, D.C., and Stryker, M.P. (1998). The role of visual experience in the development of columns in cat visual cortex. Science 279, 566–570.

Crawford, J.R., and Howell, D.C. (1998). Comparing an Individual's Test Score Against Norms Derived from Small Samples. Clin. Neuropsychol 12, 482–486.

Croydon, A., Pimperton, H., Ewing, L., Duchaine, B.C., and Pellicano, E. (2014). The Cambridge Face Memory Test for Children (CFMT-C): a new tool for measuring face recognition skills in childhood. Neuropsychologia 62, 60–67.

De Renzi, E. (1986). Prosopagnosia in two patients with CT scan evidence of damage confined to the right hemisphere. Neuropsychologia 24, 385–389.

Dehaene, S., Cohen, L., Morais, J., and Kolinsky, R. (2015). Illiterate to literate: behavioural and cerebral changes induced by reading acquisition. Nat. Rev. Neurosci. 16, 234–244.

Duncan, K.J., Pattamadilok, C., Knierim, I., and Devlin, J.T. (2009). Consistency and variability in functional localisers. Neuroimage 46, 1018–1026.

Dyer, A.G., Neumeyer, C., and Chittka, L. (2005). Honeybee (Apis mellifera) vision can discriminate between and recognise images of human faces. J. Exp. Biol. 208, 4709–4714.

Epstein, R., and Kanwisher, N. (1998). A cortical representation of the local visual environment. Nature 392, 598–601.

Farah, M.J., Rabinowitz, C., Quinn, G.E., and Liu, G.T. (2000). Early commitment of neural substrates for face recognition. Cogn. Neuropsychol. 17, 117–123.

Fedorenko, E., Hsieh, P.-J., Nieto-Castañón, A., Whitfield-Gabrieli, S., and Kanwisher, N. (2010). New method for fMRI investigations of language: defining ROIs functionally in individual subjects. J. Neurophysiol. 104, 1177–1194.

Field, D.J., Hayes, A., and Hess, R.F. (1993). Contour integration by the human visual system: evidence for a local "association field.". Vision Res. 33, 173–193.

Gabay, S., Burlingham, C., and Behrmann, M. (2014). The nature of face representations in subcortical regions. Neuropsychologia 59, 35–46.

Gauthier, I., Behrmann, M., and Tarr, M.J. (1999). Can face recognition really be dissociated from object recognition? J. Cogn. Neurosci. 11, 349–370.

Germine, L.T., Duchaine, B., and Nakayama, K. (2011). Where cognitive development and aging meet: face learning ability peaks after age 30. Cognition 118, 201–210.

Glass, L. (1969). Moiré effect from random dots. Nature 223, 578–580.

Glover, G.H. (1999). Deconvolution of impulse response in event-related BOLD fMRI. Neuroimage 9, 416–429.

Golarai, G., Ghahremani, D.G., Whitfield-Gabrieli, S., Reiss, A., Eberhardt, J.L., Gabrieli, J.D.E., and Grill-Spector, K. (2007). Differential development of high-

level visual cortex correlates with category-specific recognition memory. Nat. Neurosci. *10*, 512–522.

Greenberg, A.S., Verstynen, T., Chiu, Y.-C., Yantis, S., Schneider, W., and Behrmann, M. (2012). Visuotopic cortical connectivity underlying attention revealed with white-matter tractography. J. Neurosci. *32*, 2773–2782.

Grill-Spector, K., and Weiner, K.S. (2014). The functional architecture of the ventral temporal cortex and its role in categorization. Nat. Rev. Neurosci. *15*, 536–548.

Hadad, B.S., Maurer, D., and Lewis, T.L. (2010). The development of contour interpolation: evidence from subjective contours. J. Exp. Child Psychol. *106*, 163–176.

Hoffman, E.A., and Haxby, J.V. (2000). Distinct representations of eye gaze and identity in the distributed human neural system for face perception. Nat. Neurosci. *3*, 80–84.

Johnson, M.H. (2005). Subcortical face processing. Nat. Rev. Neurosci *6*, 766–774.

Johnson, M.H. (2011). Interactive specialization: a domain-general framework for human functional brain development? Dev. Cogn. Neurosci. *1*, 7–21.

Kanwisher, N. (2010). Functional specificity in the human brain: a window into the functional architecture of the mind. Proc. Natl. Acad. Sci. USA *107*, 11163–11170.

Kanwisher, N., McDermott, J., and Chun, M.M. (1997). The fusiform face area: a module in human extrastriate cortex specialized for face perception. J. Neurosci. *17*, 4302–4311.

Lashley, K. (1929). Brain Mechanisms and Intelligence: A Quantitative Study of Injuries to the Brain. (University of Chigago Press).

Levy, I., Hasson, U., Avidan, G., Hendler, T., and Malach, R. (2001). Center-periphery organization of human object areas. Nat. Neurosci. *4*, 533–539.

Lewis, T.L., Ellemberg, D., Maurer, D., Wilkinson, F., Wilson, H.R., Dirks, M., and Brent, H.P. (2002). Sensitivity to global form in glass patterns after early visual deprivation in humans. Vision Res. *42*, 939–948.

Liu, T.T., and Behrmann, M. (2017). Functional outcomes following lesions in visual cortex: implications for plasticity of high-level vision. Neuropsychologia *105*, 197–214.

Livingstone, M.S., Vincent, J.L., Arcaro, M.J., Srihasam, K., Schade, P.F., and Savage, T. (2017). Development of the macaque face-patch system. Nat. Commun. *8*, 14897.

Malach, R., Reppas, J.B., Benson, R.R., Kwong, K.K., Jiang, H., Kennedy, W.A., Ledden, P.J., Brady, T.J., Rosen, B.R., and Tootell, R.B. (1995). Object-related activity revealed by functional magnetic resonance imaging in human occipital cortex. Proc. Natl. Acad. Sci. USA *92*, 8135–8139.

Mancini, J., de Schonen, S., Deruelle, C., and Massoulier, A. (1994). Face recognition in children with early right or left brain damage. Dev. Med. Child Neurol. *36*, 156–166.

Mazaika, P.K., Hoeft, F., Glover, G.H., and Reiss, A.L. (2009). Methods and Software for fMRI Analysis for Clinical Subjects. Hum. Brain Mapp, 77309.

McKone, E., Crookes, K., Jeffery, L., and Dilks, D.D. (2012). A critical review of the development of face recognition: experience is less important than previously believed. Cogn. Neuropsychol. *29*, 174–212.

Nasr, S., Liu, N., Devaney, K.J., Yue, X., Rajimehr, R., Ungerleider, L.G., and Tootell, R.B.H. (2011). Scene-selective cortical regions in human and nonhuman primates. J. Neurosci. *31*, 13771–13785.

Nestor, A., Plaut, D.C., and Behrmann, M. (2016). Feature-based face representations and image reconstruction from behavioral and neural data. Proc. Natl. Acad. Sci. USA *113*, 416–421.

Ptito, A., and Leh, S.E. (2007). Neural substrates of blindsight after hemispherectomy. Neuroscientist *13*, 506–518.

Rombouts, S.A., Barkhof, F., Hoogenraad, F.G., Sprenger, M., Valk, J., and Scheltens, P. (1997). Test-retest analysis with functional MR of the activated area in the human visual cortex. AJNR Am. J. Neuroradiol. *18*, 1317–1322.

Scherf, K.S., Behrmann, M., Humphreys, K., and Luna, B. (2007). Visual category-selectivity for faces, places and objects emerges along different developmental trajectories. Dev. Sci. *10*, F15–F30.

Smith, M.A., Bair, W., and Movshon, J.A. (2002). Signals in macaque striate cortical neurons that support the perception of glass patterns. J. Neurosci. *22*, 8334–8345.

Wang, L., Mruczek, R.E.B., Arcaro, M.J., and Kastner, S. (2015). Probabilistic maps of visual topography in human cortex. Cereb. Cortex *25*, 3911–3931.

Weaver, B., and Wuensch, K.L. (2013). SPSS and SAS programs for comparing Pearson correlations and OLS regression coefficients. Behav. Res. Methods *45*, 880–895.

STAR★METHODS

KEY RESOURCES TABLE

REAGENT or RESOURCE	SOURCE	IDENTIFIER
Deposited Data		
Raw behavioral and fMRI data	KiltHub (https://kilthub.cmu.edu), which is a part of figshare (https://figshare.com)	https://figshare.com/articles/Successful_Reorganization_of_Category-Selective_Visual_Cortex_Following_Occipito-Temporal_Lobectomy_in_Childhood/5919409/1
Experimental Models: Organisms/Strains		
Human: patient, controls	Children's Hospital of Pittsburgh, Pittsburgh, USA	N/A
Software and Algorithms		
BrainVoyager QX 2.8.2	Brain Innovation, Maastricht, Netherlands	http://www.brainvoyager.com/
Freesurfer	Laboratory for Computational Neuroimaging, Athinoula A. Martinos Center for Biomedical Imaging, Boston, USA	https://surfer.nmr.mgh.harvard.edu/
MATLAB, 2014	MathWorks	https://www.mathworks.com
Psychtoolbox	N/A	http://www.psychtoolbox.org
Neuroelf toolbox	N/A	http://neuroelf.net/
SPM 8	Wellcome Department of Cognitive Neurology, London, United Kingdom	http://www.fil.ion.ucl.ac.uk/spm/software/spm8/
ArtRepair toolbox	Mazaika et al. (2009)	http://cibsr.stanford.edu/tools/human-brain-project/artrepair-software.html
R	The R Foundation	https://www.r-project.org/

CONTACT FOR REAGENT AND RESOURCE SHARING

Further information and requests for resources should be directed to and will be fulfilled by the Lead Contact, Marlene Behrmann (behrmann@cmu.edu).

EXPERIMENTAL MODEL AND SUBJECT DETAILS

Patient

Patient U.D., a young male with pharmacologically intractable epilepsy was of normal health and cognitive abilities until age 4 when he suffered his first seizure, a result of a low-grade brain tumor in the right posterior temporal lobe (Figure 1A, Top). The surgical procedure, conducted at age 6 years 9 months, resulted in the removal of the entire occipital lobe and roughly three quarters of the temporal lobe posteriorly in the RH (Figure 1A, Bottom). On post-operative testing, U.D. showed age-appropriate intellect and language skills (see Table S2). Despite the dense left homonymous hemianopia (Figure 1C), U.D. demonstrated normal performance on tasks such as glass pattern perception (Lewis et al., 2002) and contour integration (Hadad et al., 2010), and he showed normal recognition of faces (Croydon et al., 2014) and objects (Gauthier et al., 1999) (Table S1). Left hemisphere (LH) language dominance remained unchanged from pre- to post-surgery, as revealed using fMRI (see Figure S1 for more details).

Post-surgery, U.D. continued to function at an above average intellectual level: (1) General intellectual function: pre-surgical IQ is 116 and post-surgical IQ is 118; (2) Scholastic performance: standardized school assessment/PSSA scores are in the proficient-to-advanced range at age 9-10; (3) School and family support: U.D. receives vision therapy and various accommodations at school as a result of the dense hemianopia, such as preferential seating on the left of the room and access to enlarged print when needed. He has a very supportive family. U.D. and his parents provided assent and informed consent in compliance with the protocol approved by the Institutional Review Board of Carnegie Mellon University (CMU) and the University of Pittsburgh.

During the 3 years of this investigation (age 7y10m - 10y10m), U.D. participated in five separate fMRI sessions and two separate behavioral testing sessions (see Figure 1D for the timeline of the investigation). The first three category localizer (CL) sessions were conducted roughly six months apart (CL1: 7y 10 m, CL2: 8y4m, CL3: 8y10m) and an additional scan was conducted at age 10y10m

(CL4). The same retinotopic mapping (RM) task was used for RM1 and RM2, at 9y and 10y10m respectively. Two behavioral testing (BT) sessions, BT1 and BT2 (9y, 10y10m), were conducted at the same time as RM1 and RM2.

Controls

To evaluate whether the observed change in U.D. over time reflects the normal developmental profile or some altered form of plasticity, 11 age-matched control subjects (right-handed, 7 male, 7-11 years old) participated in the fMRI studies. Based on the conservative motion parameters we adopted, 7 out of 30 category localizer runs were discarded due to excessive motion (> 1.5 mm translation or > 1.5° rotation). Thus, the CL analysis included a total of 8 control participants (23 runs).

Eight of the 11 fMRI subjects also participated in the behavioral testing study (on a different day within a week). An additional group of 7 age-matched control subjects (right-handed, 4 male, 7-10 years old) participated in the behavioral testing. One of these 15 participants was excluded as an outlier (performance was 2 SD outside mean), leaving 14 control participants in the BT study.

All participants had normal or corrected-to-normal visual acuity and no history of neurological disorder. The children and their parents provided assent and informed consent to participate in the protocol approved by the Institutional Review Board of Carnegie Mellon University and the University of Pittsburgh.

METHOD DETAILS

Stimuli and Procedures
Behavioral experiments (outside scanner)
Measurement of visual perception was conducted twice in U.D. (BT1: 9y, BT2: 10y10m) and once in the 14 controls (right-handed, 9 male, 7-11 years old) using the same computer with similar viewing distances (about 60 cm). Each testing session consisted of two sections: the first section evaluated global form perception and the second focused on more complex pattern recognition.
Section 1: Global form perception
The perception of shape or global form was assessed using thresholds derived from a Glass pattern (Glass, 1969) and a contour integration (Hadad et al., 2010) task. The perception of Glass patterns is thought to be achieved by lateral connections in V1/V2 neurons (Smith et al., 2002) and contour integration is thought to tap into longer-range interactions in V1-V3 (Field et al., 1993).
Glass Patterns.   In the Glass patterns experiment, we varied the percentage of signal dots (Lewis et al., 2002) using a 1-up (after incorrect response), 3-down (after 3 correct responses) adaptive staircase method to measure the 75% threshold for detecting the concentric swirl (Figure S5A). The staircase started at 95% signal. It terminated after 10 reversals, and the threshold was measured from the geometric mean of the last 6 reversals. Each Glass pattern was centrally presented and extended about 8.57° horizontally and 8.56° vertically. U.D.'s performance in each behavioral session was compared to that of the 14 age-matched controls.
Contour Integration.   The contour integration task used two collinearity conditions from Hadad et al. (2010): target gabor elements had either ± 20° or ± 0° collinearity, and the participant was asked to indicate whether an embedded egg-like shape pointed to the right or left (Figure S5B). Background elements were varied according to a 1-up (after a wrong response), 3-down (after 3 correct responses) staircase procedure, and the experiment continued until 10 reversals in the staircase occurred. The threshold score was calculated from the geometrical mean spacing of the final 6 reversals. The active display (that contained gabor elements) extended about 17.6° horizontally and 12.6° vertically. U.D.'s performance in each behavioral session was compared to that of the 14 age-matched controls.
Section 2: Pattern recognition
Face Recognition.   We used the Cambridge Face Memory Test (CFMT-C) (Croydon et al., 2014) for children (see Figure S5C for stimuli and procedures). Participants studied a set of 5 faces and then, in subsequent trials, identified the 'old' faces from among new, distractor faces. The test was conducted for both upright and inverted faces. Each face was centrally presented and extended about 3.4° horizontally and 4.9° vertically. There were 60 trials in each orientation: 15 introductory trials, 25 trials without noise, and 20 with noise. Performance was the total percent correct out of 60 trials, separately for the upright and inverted version. U.D.'s face recognition performance was compared to that of the standardized age-appropriate norms.
Object Recognition.   In this task (adapted from Gauthier et al., 1999), two objects were presented simultaneously — one above and one below the midline of the screen to accommodate the patient's hemianopia — for same/different discrimination. When the objects differed, they could differ at the basic (duck versus vehicle), subordinate (chair versus piano), or exemplar level (table 1 versus table 2; see Figure S5D for examples). The task consisted of 100 trials, 40 same and 60 different (twenty per level). Same and different trials (all levels) were randomly intermixed. The display remained visible until response with one key to indicate 'same' and another key for 'different'. Each object extended about 7.3° horizontally and 6.9° vertically. U.D.'s object recognition performance in each behavioral session was compared to that of the 14 age-matched controls.
Behavioral tasks (inside scanner)
The visual presentations were generated using MATLAB (The MathWorks, Natick, MA) and Psychtoolbox (http://psychtoolbox.org). Images were back-projected onto a screen located in the bore of the scanner (visual angle = 16°). A trigger pulse from the scanner synchronized the onset of the stimulus presentation to the beginning of the image acquisition. Participants were instructed to maintain fixation during all the functional runs. During the Retinotopic Mapping (RM) and the Category Localizer (CL) tasks, a central

fixation dot remained on the screen to orient participants' eye fixation, and eye movements were monitored during the scan using an ASL eye tracker (Applied Science Laboratories, Billerica, MA). Analysis of eye positions confirmed that U.D. was able to maintain fixation within $\pm 2°$ of visual angle from the center of the screen during both tasks (excluding blinks, gaze deviation from center in horizontal position: $1.64° \pm 0.12°$, gaze deviation from center in vertical position: $1.06° \pm 0.15°$) and each session was within the control range (horizontal: all $t < 0.224$, all $p > 0.829$; vertical: all $t < 0.415$, all $p > 0.691$, Crawford's modified t test). Next, analysis of gaze deviation across categories revealed no systematic differences in CL1, 3, or 4 (all $F < 1.640$, all $p > 0.154$, one-way repeated-measures ANOVA), suggesting stable fixation profiles and encoding strategy. In addition, performance was close to ceiling (accuracy: $94 \pm 3.7\%$) in the CL tasks and the absence of a behavioral response to the LVF stimuli in the RM tasks suggest that U.D. was compliant and was able to maintain fixation.

fMRI Experiments

Pre- and post-surgical language localizer

Approximately 3 months prior to surgery, language regions were localized using a verb generation task on a 3T GE Medical Systems MR scanner in the hospital (LL1 in Figure 1D). In the first fMRI session post-surgically (LL2 in Figure 1D), a language localizer task (Fedorenko et al., 2010) was conducted at CMU. Full details of the tasks are available below and a comparison of pre- versus post-surgical language localizer results are shown in Figure S1. As expected and confirmed, there were no obvious changes in the left hemisphere language dominance from the pre- to post-surgery scan.

Pre-surgical (clinical) language localizer

A clinical verb generation task was performed using a 3T GE Medical Systems MR scanner in the hospital, approximately 3 month before the surgery. This task adopted a block design with 5 repeats of random noise block and nouns block, and this language localizer lasted 5 min in total. The task was to generate a verb in response to the presented noun. In Figure S1A, normal activation for verb generation is seen with left-hemisphere dominance. Activation was present in the left inferior frontal gyrus (left IFG, BA 44; Broca's area) as well as in the left posterior superior temporal gyrus and caudate).

Post-surgical (functional) language localizer

On the first fMRI session post-surgically, a language localizer task (Fedorenko et al., 2010) was conducted at CMU. The stimuli used in the block design consisted of two categories: sentences and nonword strings. Participants were instructed to press one button (index finger) to indicate if the blue word/nonword shown immediately after the sequence (9 words/nonwords) matched one of the words/nonwords in this sequence, and another button (middle finger) to indicate a non-match. This response instruction was designed to maximally engage participants while keeping the task relatively easy. The target length of this experiment was two runs. Standard general linear model (GLM) analyses were run with 3 predictors (sentences, nonword strings, fixations), each convolved with a canonical hemodynamic response function (Glover, 1999). Language-selective ROIs were determined using the sentences-nonwords or sentences-fixation contrast. Using this task, we confirmed the left hemisphere dominance (left IFG activation) in U.D. post-operatively.

Category localizer (CL)

The one-back fMRI localizer task (Nestor et al., 2016) adopted a block design with stimuli from 5 categories (Figure 2A): faces, houses, objects, scrambled objects, and words. Each run consisted of 3 repeats of each category in pseudorandom order with a fixation baseline between all stimulus conditions. Thus, each run contained 15 conditions and 16 fixation baselines and lasted 6min8s in total. Participants were instructed to indicate an immediately repeating image among 16 images per block (a one-back task) and responses were made using the right index finger via a MR compatible button glove. This response instruction was designed to engage participants maximally while keeping the task relatively easy for the children (performance was at ceiling, e.g., accuracy: $94 \pm 3.7\%$).

Retinotopic mapping (RM)

Retinotopic regions were demarcated using a meridian mapping task (adapted from Greenberg et al., 2012). A flickering checkerboard wedge was presented in each quadrant of the visual fields to map separate representations of the contralateral and ipsilateral upper and lower visual space (Figure 5A). Each run lasted 3min56s in total, and contained three repeats of all four visual field conditions in a fixed order with two fixation baselines at the beginning and end of each run. The task required a button press to indicate a change in color at central fixation. Maintaining fixation throughout the run was emphasized prior to the experiment. There were 4 runs collected in RM1 and 2 runs in RM2 (time permitting). Using all 4 runs or the two best runs in RM1 (matched to the number of runs in RM2) did not have a noticeable impact on the retinotopic maps.

Scanning

MRI data were acquired on a Siemens Verio 3T magnet at the Scientific Imaging and Brain Research Center at CMU, using a 32-channel phased array head coil. Prior to the experiment, 8 out of 10 control participants with no prior MRI experience participated in a practice session in a mock scanner to acclimate to the experimental conditions, and a head tracker was used to minimize head motion. U.D. had been scanned in the hospital multiple times previously so we did not subject him to the simulation conditions. All participants performed a practice version of the experimental tasks outside the scanner to gain familiarity with the procedure.

Structural MRI

A high-resolution (1mm^3 isotropic voxels, 176 sagittal slices, acquisition matrix = 256 × 256, TR = 2300 ms, TE = 1.97 ms, inversion time = 900 ms, flip angle = 9°, GRAPPA = 2, scan time = 5min21s) T1-weighted whole brain image was acquired for each participant (and for each session in U.D.) using a magnetization prepared rapid gradient echo imaging (MPRAGE) sequence for localization, co-registration and surface reconstruction purposes.

Functional MRI

In patient U.D. and two 9-year-old controls, fMRI data were collected with a BOLD contrast sensitive echo planar imaging (EPI) sequence (TR = 2000ms, TE = 30ms, voxel size = 2.5mm^3, flip angle = 79°, GRAPPA = 2). Slice prescriptions were AC-PC aligned. In the other 8 controls, fMRI data with whole brain coverage were collected with multiband acceleration factor of 3 and voxel size = 2 mm^3 (all else equal to standard protocol used in U.D. and tSNRs were not significantly different between the two control groups). To ensure accurate within-subject comparison, we co-registered all localizer runs in U.D. to the structural MRI from the first session and, for all participants, carefully monitored the head motion and the tSNR across sessions (Figure 2D-F).

QUANTIFICATION AND STATISTICAL ANALYSIS

fMRI Data Analysis
Preprocessing
MRI data were preprocessed using BrainVoyager QX (Brain Innovation, Maastricht, the Netherlands). Preprocessing of the anatomical MRI included brain extraction/skull stripping, intensity inhomogeneity correction, and AC-PC alignment (and/or Talairach transformation). Segmentation and surface reconstruction was achieved using a combination of BrainVoyager and Freesurfer with manual correction of the white matter tree. Conversion between BrainVoyager and Freesurfer was achieved via the NIfTI conversion plugin available in Brainvoyager.

CL data were 3D-motion corrected (trilinear/sinc interpolation) and temporally filtered (high-pass GLM fourier = 2 cycles). RM data were 3D-motion corrected (sinc interpolation), temporally filtered (high-pass GLM fourier = 2 cycles), and slice timing corrected (cubic spline; multiband: slice order according to acquisition time). Despiking of high-motion time points was performed using the ArtRepair toolbox (Mazaika et al., 2009) in Statistical Parametric Mapping (SPM, www.fil.ion.ucl.ac.uk/spm/). Despiking improves tSNR by reducing the standard deviation of the noise in the time series (see tSNR equation). Conversion between BrainVoyager and SPM was achieved via Neuroelf toolbox (http://neuroelf.net/) in MATLAB. Functional data were not spatially normalized.

Head motion
During each functional run in each subject, the amount of head motion was calculated from the combination of three translation parameters (in millimeters) and three rotation parameters (in degrees) using the equations below. This led to the exclusion of 3 of the 11 controls (7 out of 30 CL runs) and 7 out of 15 CL runs in patient U.D. (criterion: excessive motion: > 1.5 mm translation or > 1.5° rotation). Thus, 3 runs in each of the eight controls (except 2 runs in S7) were included in the analysis. In U.D., there were 8 runs included in the analyses, consisting of 1 run in CL1, 2 runs in CL2 and CL3, and 3 runs in CL4. The average head motion was not significantly different in each session in U.D. (translation: 0.54 ± 0.28, rotation: 0.54 ± 0.22) compared to controls (translation: 0.48 ± 0.39 mm, rotation: 0.50 ± 0.33 degree) (Crawford's modified t test for single-case studies: all t values < 0.52, all p values > 0.618, Figure 2D).

$$\text{Total translation} = \sqrt{d(x)^2 + d(y)^2 + d(z)^2}$$

$$\text{Total rotation} = \sqrt{r(x)^2 + r(y)^2 + r(z)^2}$$

tSNR
To ensure that any comparisons across sessions in U.D. and between U.D. and the controls were not merely the consequence of differences in the quality of the individual scan, we used tSNR as the metric to compare fMRI data quality. tSNR represents the SNR of the timeseries at each voxel. For each run, tSNR was calculated as the mean signal of the fMRI time series divided by the standard deviation of the noise in the time series:

$$\text{tSNR}_{(temporal)} = \mu_{timeseries} / \sigma_{timeseries}$$

Whole-brain global tSNR and local tSNR just of the left VOTC region (remote from the lesion but the critical region where change in topography was observed) were calculated for each control and each session in U.D. The average whole-brain global tSNR across voxels was not significantly different between each session in U.D. (Figure 2F, one-way ANOVA: F = 0.32, p > 0.81) and the controls (Figure 2E, Crawford's modified t test for single-case studies: all t values < 0.06, all p values > 0.96). In addition, local tSNR statistics for the anatomically defined left FG+OTS regions showed that each session in U.D. was within the distribution of controls (Crawford's modified t test for single-case studies: all t values < 0. 38, all p values > 0.72).

General linear model (GLM)

For each run, a standard GLM was performed. In both CL and RM datasets, a regressor for each condition was defined as a boxcar function convolved with a canonical hemodynamic response function (Glover, 1999). CL regressors included faces, houses, objects, scrambled objects and words. Fixation conditions were not included to avoid overfitting. RM regressors included LVF, right visual field (RVF), upper visual field, lower visual field and fixation. Fixation conditions were included in RM for both the LVF-minus-fixation (U.D. has left hemianopia) and for the RVF-minus-fixation contrast.

In CL, several GLM analyses were conducted for each control and each session in U.D.: (1) data from all runs were used to visualize category-selective activation (Figure 2) and quantify the extent of activation (Figure S2), (2) data from the first run in each control and the first run in U.D.'s CL4 were used to define category-selective ROIs, (3) independent data from the remaining run(s) were used to quantify the magnitude of the category selectivity (Figure 3). In the RM analysis, the GLM analysis generated statistical t-maps and contrast values corresponding to differences visual fields (Figures 5 and S4).

Functional ROI definition

Category-selective ROIs were defined as a contiguous cluster that was robust at a threshold of $t > 3$ (voxel level) under each weighted contrast (a category of interest – all other categories), thereby controlling for any differences in low-level image features and raw signal strength in each session. The topography in the controls consisted of bilateral face-selective activation in the FFA and STS; bilateral scene-selective activation in the PPA and TOS; bilateral object-selective activation in the LOC, and left-lateralized word-selective activation in the VWFA. Although note that not every control showed face or word activation at the individual level, as is standard in children. Also note that the FFA refers to the combination of FFA1/posterior fusiform (pFus)-faces and FFA2/mid fusiform (mFus)-faces throughout the paper unless otherwise specified. In U.D., due to resection encompassing the right VOTC, most of the category-selective responses in U.D. were confined to the LH, including lFFA, lSTS, lPPA, lTOS, lLOC, and VWFA.

To avoid selection bias resulting from using the same data to select the regions and then quantify the selectivity, in U.D., the first run in CL4 was used to define category-selective ROIs and the rest of the data (1 run in CL1, 2 runs each in CL2-4) were used to quantify selectivity. In each control, we defined the category-selective ROIs using data from the first run and then used independent data from the remaining two runs (except only one run for S7) to derive mean category selectivity.

Retinotopic ROIs were defined based on the reversal of horizontal and vertical meridians. In each subject, V1 was identified as the cluster of activated voxels in the calcarine sulcus of each hemisphere between the upper and lower representation of the vertical meridian. The V2/V3 ROI was identified as the clusters immediately ventral/dorsal to the representation of the vertical/horizontal meridian.

Anatomical ROI definition

The outlines of the fusiform gyrus (FG) (including the mid-fusiform sulcus) and the occipitotemporal sulcus (OTS) were first hand-drawn in surface space (Figure 4A) and then converted to volume space (Figure 4B). The same method was applied to a control anatomical ROI, LO2 (Wang et al., 2015) (Figure S3A–S3B). The face-minus-word response in each voxel within the FG+OTS region (Figure 4C) is depicted in t score [$t_{(face-word)}$].

Comparison between patient and controls

In the analyses on the topography and magnitude of selectivity, U.D. was compared to the control group using two statistical approaches. First, Crawford's modified t test (Crawford and Howell, 1998) was used for between-subject analyses comparing U.D. and controls. The reported t scores and p values are under the two-tailed test throughout the paper. Second, methods for comparing two independent regression coefficients with unpooled variance (Weaver and Wuensch, 2013) were used to assess differences in the regression slopes between U.D.'s and controls' (Figures 3 and S2).

Dice coefficient

Dice coefficient (Rombouts et al., 1997) was used as the measure of reproducibility of the size and the location of the activation across CL sessions in U.D. It is calculated by the following equation:

$$R_{overlap} = 2(V_{overlap}) / (V_A + V_B).$$

In the Dice equation, $V_{overlap}$ is the number of voxels that overlap between session A and B. The denominator is the total number of significant voxels in the two sessions. The Dice coefficient varies between 0.0 (no reproducibility) and 1.0 (perfect reproducibility). Given that Dice coefficients are highly dependent on the statistical threshold (Duncan et al., 2009), the number of voxels included in each session was systematically varied until the best average pairwise Dice coefficients was obtained for each category-selective patch.

Representational similarity analysis (RSA)

RSA was used to characterize multivariate response patterns by means of a representational dissimilarity matrix (RDM, Figures 4D and S3C). Input to the RDM were 16 volume maps [4 (category) x 4 (CL session)] containing results from overlaying a t-map for each condition (e.g., "Face 1," "Face 2," … "Object 1"). Pearson correlation coefficient (r) was first calculated and the resulting r ranged from −1.0 (perfect negative correlation) over 0.0 (no correlation) to +1.0 (perfect positive correlation). The correlation coefficient (r) was then transformed to dissimilarity (d) by applying the equation: d = 1 − r.

A multi-dimensional scaling (MDS) algorithm (MATLAB function: cmdscale) was run on the dissimilarity values stored in the upper (or equivalently the lower) triangle of the RDM. The resulting MDS plot visualizes the similarity structure coded in the RDM as distances between conditions in a two-dimensional representation (Figures 4E and S3D).

Based on the dissimilarity value between face and word in each session in the RDM, a regression slope was derived as an index of change between their representations. Another regression slope of the dissimilarity value between house and object in each session was calculated to capture the relationship between house and object representation over time. Bootstrapped regression slopes were calculated from the randomly picked 4 values (as a proxy for 4 sessions) after shuffling the condition labels in the upper (or equivalently the lower) RDM. This analysis yielded a distribution of the bootstrapped regression slopes (cyan histogram in Figure 4F), and the face and word dissimilarity slope (red dot in Figure 4F) and the house and object dissimilarity slope (yellow dot in Figure 4F) was each compared with this null distribution. To establish the statistical significance of the difference between bootstrapped slopes and the face and word dissimilarity slope or the house and object dissimilarity slope, we calculated the 95% CI of the obtained bootstrap distribution of the mean. For comparison, see RSA on a control anatomical region (LO2) in Figure S3.

DATA AND SOFTWARE AVAILABILITY

Behavioral and fMRI data and experiment scripts are available on KiltHub, which is a part of figshare (https://figshare.com/articles/Successful_Reorganization_of_Category-Selective_Visual_Cortex_Following_Occipito-Temporal_Lobectomy_in_Childhood/5919409/1).

Supplemental Information

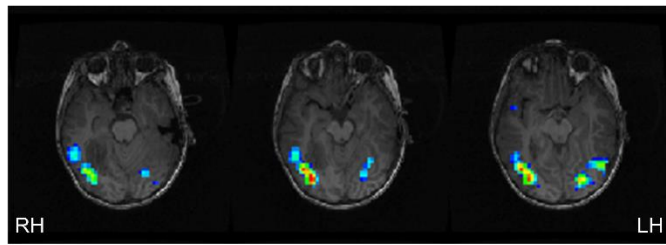## Successful Reorganization of Category-Selective

Visual Cortex following Occipito-temporal
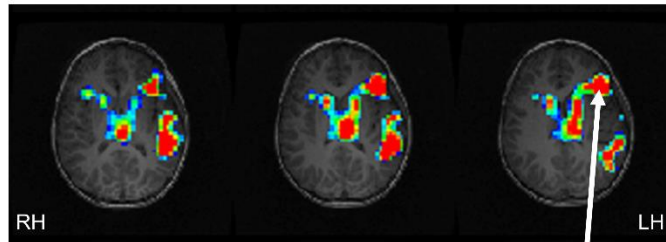
Lobectomy in Childhood

Tina T. Liu, Adrian Nestor, Mark D. Vida, John A. Pyles, Christina Patterson, Ying Yang, Fan Nils Yang, Erez Freud, and Marlene Behrmann

A.

1. Visual task:
(spinning circle - crosshair)

RH   LH

2. Verb generation task:
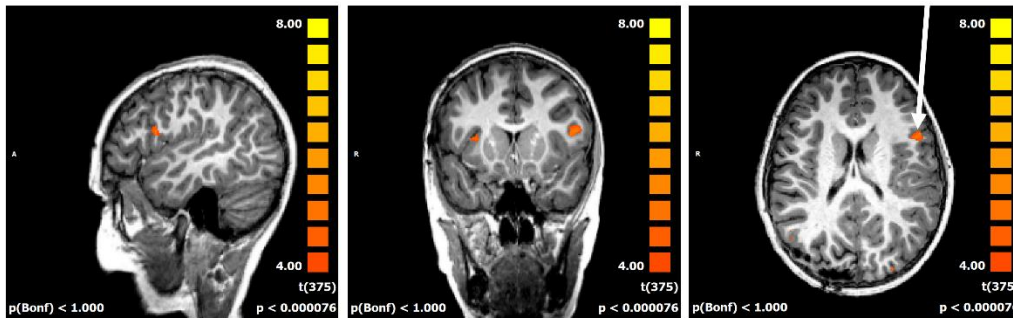(nouns – random noise)

RH   LH

B.

Figure S1. Pre- and post-surgical language mapping results. Related to Figure 1.
(A) Tasks and results from the pre-surgical clinical/functional localizer: (1) visual task and (2) language/verb generation task.
(B) Results from the post-surgical language localizer (Fedorenko et al., 2010).
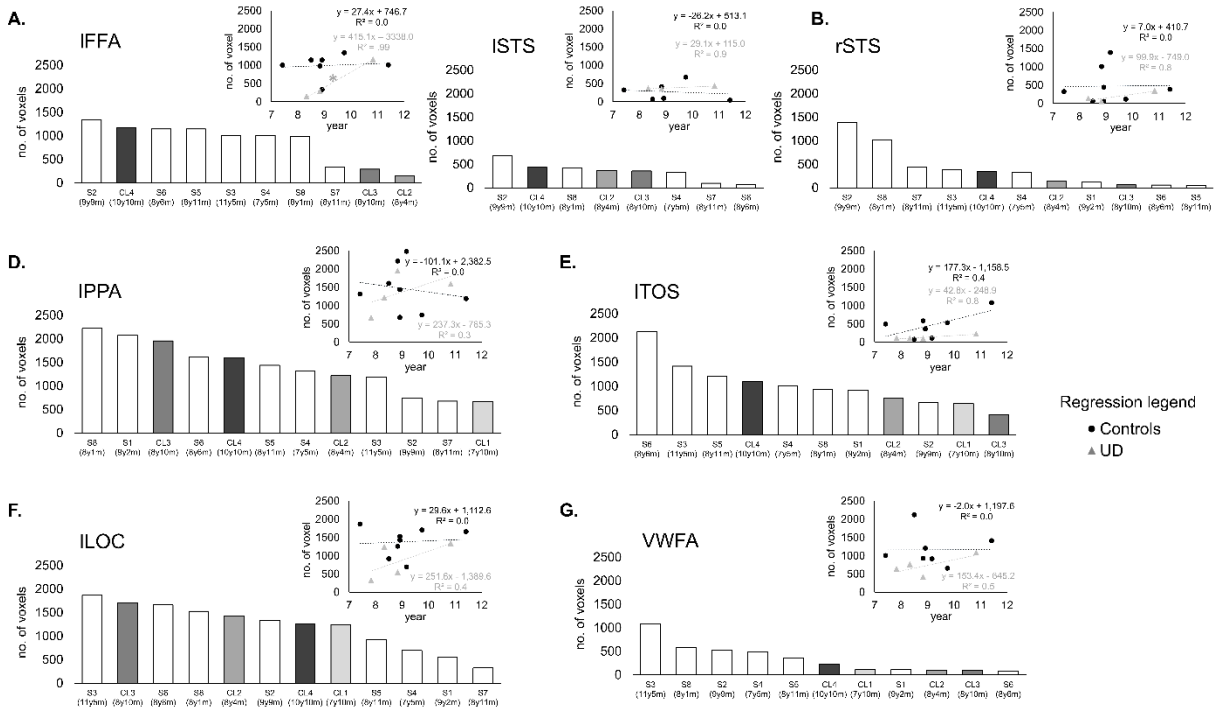
Figure S2. Extent of activation in controls and UD in A) IFFA, B) ISTS, C) rSTS, D) IPPA, E) ITOS, F) ILOC, and G) VWFA. Related to Figures 2 and 3.

Bar chart (main figure): Number of voxels in individual controls (white) and UD (different shades of grey for different sessions). Each white bar reflects data from a single control participant. The X-axis is ranked in descending order of age to indicate where UD falls in the control distribution.

Scatter plot (secondary figure, top right corner): Linear regression showing the relationship between age (X-axis) and the extent of activation (Y-axis: number of voxels) in the controls (black dots, regression lines, equations and R-squared values) and in UD (grey triangles, regression lines, equations and R-squared values). An asterisk (dark grey) is above the slope when there is a significant linear relationship (IFFA).

The number of regions defined in controls[1]: IFFA (n=7), ISTS (n=5), rSTS (n=8), IPPA (n=8), ITOS (n=7), ILOC (n=8), and VWFA (n=7).

---

[1] Note that here the regions were defined using all available runs, whereas the ROIs used to quantify the magnitude of selectivity were defined from the first run in each subject.
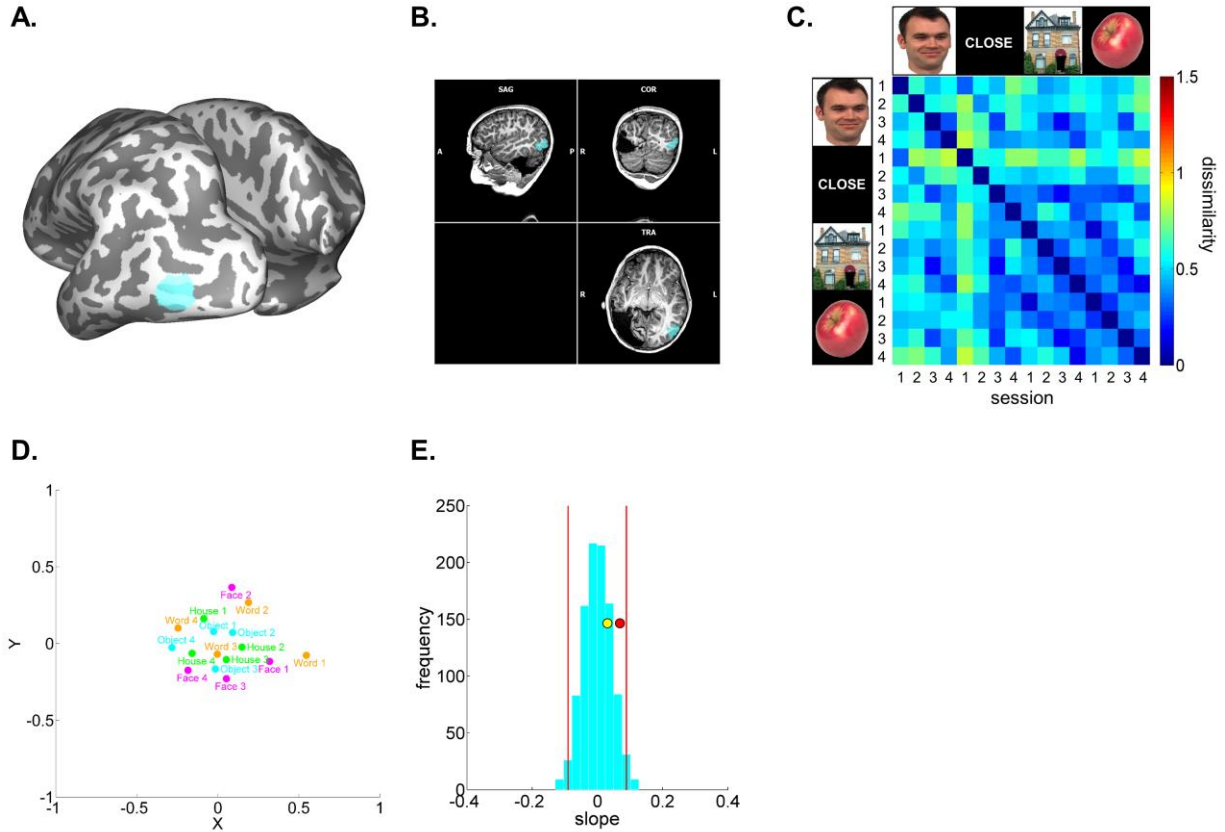
Figure S3. Results from the control anatomical ROI (LO2) analysis. Related to Figure 4.
(A) LO2 (cyan) in the surface space (based on LO2 in Wang et al. 2015).
(B) LO2 (cyan) in the corresponding volume space.
(C) Representational dissimilarity of category representations across sessions in the LO2 region.
(D) MDS plot of category representations across sessions in the LO2 region. Orange: words, Pink: faces, Green: houses, Blue: objects.
(E) A distribution of bootstrapped dissimilarity slopes (cyan histogram), face and word dissimilarity slope (red dot), and house and object dissimilarity slope (yellow dot) as a function of session. Red vertical lines represent 95% CI.
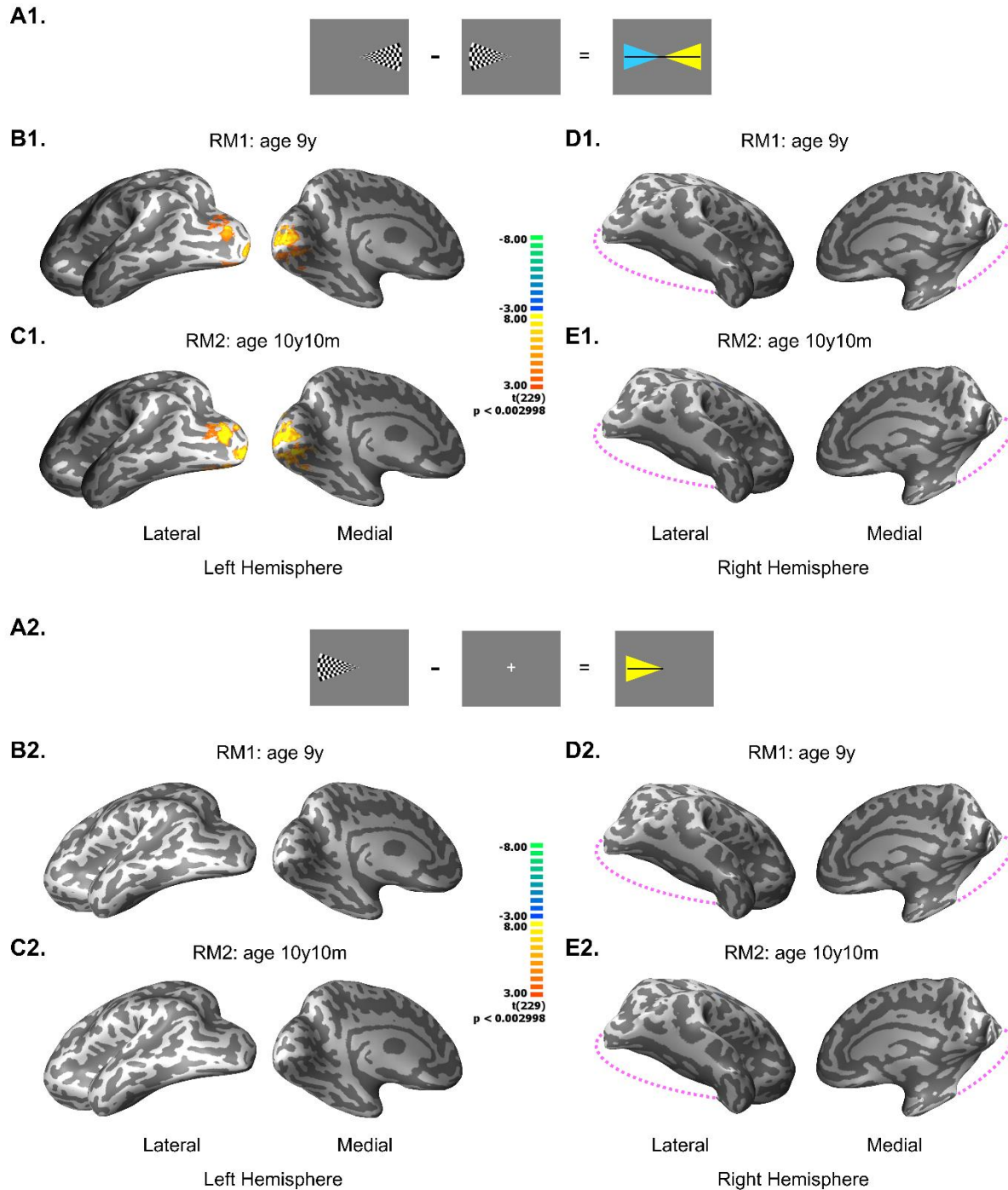
Figure S4. Early visual cortex activation under the RVF-LVF contrast (A1-E1) and the LVF-fixation contrast (A2-E2) in the left and right hemispheres of UD in RM1 (age 9y) and RM2 (age 10y10m). Related to Figure 5.
(A1) Stimuli and contrasts used in the retinotopic mapping experiment. This image shows a contrast between RVF and LVF (RVF-LVF).
(B2) Retinotopic response in the LH in RM1 (age 9y).
(C2) Retinotopic response in the LH in RM2 (age 10y10m).

(D2) Retinotopic response in the RH in RM1 (age 9y).
(E2) Retinotopic response in the RH in RM2 (age 10y10m).
Stronger responses to stimulation in the RVF are shown in yellow and orange, stronger responses to stimulation in the LVF are shown in blue and green. Color scale bars represent t scores. Note that no activation was found in the RH as reflected by a lack of retinotopic response under the RVF-LVF contrast.
(A2) Stimuli and contrasts used in the retinotopic mapping experiment. This image shows a contrast between LVF and fixation (LVF-fixation).
(B2) Retinotopic response in the LH in RM1 (age 9y).
(C2) Retinotopic response in the LH in RM2 (age 10y10m).
(D2) Retinotopic response in the RH in RM1 (age 9y).
(E2) Retinotopic response in the RH in RM2 (age 10y10m).
Stronger responses to stimulation in the LVF are shown in yellow and orange, stronger responses to stimulation in the fixation are shown in blue and green. Color scale bars represent t scores. Note that no activation was found in either hemisphere reflecting a lack of retinotopic response under the LVF-fixation contrast.
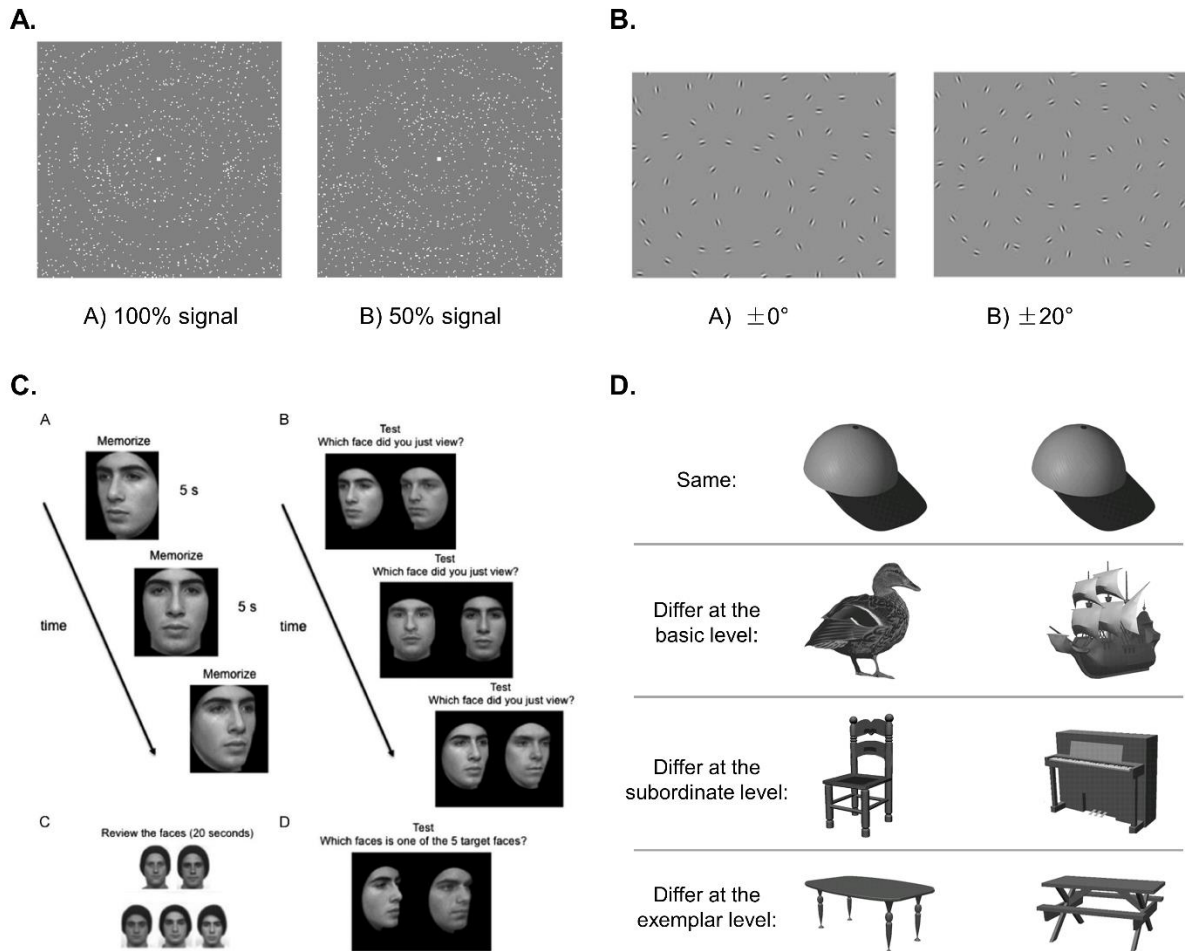
Figure S5. Examples of stimuli in the behavioral experiments. Related to Figure 1.

(A) Glass pattern (Lewis et al., 2002). Participants viewed two sequentially displayed patterns and pressed a button to indicate which display had more concentric swirl.

(B) Contour integration (Hadad et al., 2010). Participants viewed a brief presentation and indicated the leftward or rightward pointing of the embedded "egg-like" shape.

(C) CFMT-C (Croydon et al., 2014). Participants were instructed to remember a set of target faces and identify them amongst distractor faces.

(D) Object Matching Experiment (Gauthier et al., 1999). Participants made same/different discrimination on pairs of objects.

Table S1. Behavioral results of visual perceptual performance in UD and age-matched controls. Related to Figure 1.

		Participant	Age	Version	Threshold	
Intermediate-level vision	Contour integration[1]	Patient	9y	±0 collinearity	57.51	
			9y	±20 collinearity	76.97	
			10y10m	±0 collinearity	51.96	
			10y10m	±20 collinearity	76.88	
		Control[1]	7-11y (n=14)	±0 collinearity	60.12 (9.09)	
			7-11y (n=14)	±20 collinearity	74.95 (4.69)	
		Participant	**Age**	**Threshold (1st time)**	**Threshold (2nd time)**	**Average Threshold**
	Glass pattern[1]	Patient	9y	33.33	34.17	33.75 (0.59)
			10y10m	25.83	27.5	26.67 (1.18)
		Control[1]	7-11y (n=14)	49.52 (8.58)	41.31 (7.13)	45.42 (6.53)
		Participant	**Age**	**Version**	**Total % correct**	
High-level vision	CFMT-C[2]	Patient	9y	upright	76.67	
			9y	inverted	58.33	
			10y10m	upright	83.33	
			10y10m	inverted	68.33	
		Control[2]	9y (n=33)	upright	81.6 (9.0)	
			9y (n=33)	inverted	67.9 (6.1)	
			11y (n=29)	upright	83.2 (9.2)	
			11y (n=29)	inverted	74.2 (9.1)	
		Participant	**Age**	**Accuracy (% correct)**	**RT (ms)**	**Inverse efficiency**
	Object Matching[1]	Patient	9y	89	993.99	1116.84
			10y10m	91	1366.96	1502.15
		Control[1]	7-11y (n=14)	88.57 (5.9)	1218.29 (338.17)	1366.42 (320.95)

[1] Each age-matched control participated in all of the three following tests: Object Matching, Contour Integration, and Glass Pattern.
[2] CFMT-C control scores per age group were based on those from the typical developing children reported in (Croydon et al., 2014).

Table S2. Summary of UD's scholastic performance and neuropsychological evaluation test performance before and after the surgery. Related to Figure 1.

Scholastic performance						
Woodcock-Johnson – III Test of Achievement (Pre-surgery)				Pennsylvania Systems of School Assessment (Post-surgery)		
Subject	Reading	Letter-Word	Passage	Subject	English Language Arts	Mathematics
Percentile	63rd	67th	56th	Standard score[1]	1028/1586	1094/1594
				Evaluation	Proficient	Proficient

General Intellectual Function Wechsler Abbreviated Scales of Intelligence (WASI-2)						
	Pre-surgery			Post-surgery		
Indices	Full Scale	Verbal	Performance	Full Scale	Verbal	Performance
Standard score[1]	116	135	97	118	123	108
Descriptive	High average	Very superior	Average	Superior	Superior	Average

Language						
	WASI-2 (Pre-surgery)			NEPSY-II (Post-surgery)		
Subtest	Vocabulary			Subtest	Comprehension	Semantic	Phonemic
Scaled score[2]	15			Scaled score[2]	11	17	17
Descriptive	High average			Percentile	63rd	99th	99th

Fine Motor/ Visual-Motor Integration Grooved Pegboard				
	Pre-surgery		Post-surgery	
Hand	Dominant Hand (RH)	Nondominant Hand (LH)	Dominant Hand (RH)	Nondominant hand (LH)
Time	97"	51"	38"	50"
Percentile	7th	53rd	50th	26th

Executive Control Processes Wechsler Intelligence Scale for Children (WISC-V)				
	Pre-surgery		Post-surgery	
Indices	Working Memory	Processing Speed	Working Memory	Processing Speed
Standard score[1]	80	106	94	95
Percentile	9th	66th	34th	37th
Descriptive	Weak	Average	Average	Average

[1] Standard score: Mean =100, Standard Deviation = 15
[2] Scaled score: Mean = 10, Standard Deviation = 3